

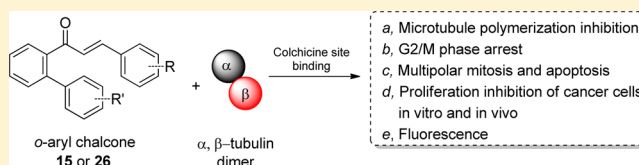
Discovery of Potent Cytotoxic Ortho-Aryl Chalcones as New Scaffold Targeting Tubulin and Mitosis with Affinity-Based Fluorescence

Cuige Zhu,[†] Yinglin Zuo,[†] Ruimin Wang, Baoxia Liang, Xin Yue, Gesi Wen, Nana Shang, Lei Huang, Yu Chen, Jun Du, and Xianzhang Bu*

School of Pharmaceutical Sciences, Sun Yat-Sen University, Guangzhou 510006, China

Supporting Information

ABSTRACT: A series of new ortho-aryl chalcones have been designed and synthesized. Many of these compounds were found to exhibit significant antiproliferation activity toward a panel of cancer cell lines. Selected compounds show potent cytotoxicity against several drug resistant cell lines including paclitaxel (Taxol) resistant human ovarian carcinoma cells, vincristine resistant human ileocecum carcinoma cells, and doxorubicin resistant human breast carcinoma cells. Further investigation revealed that active analogues could inhibit the microtubule polymerization by binding to colchicine site and thus induce multipolar mitosis, G₂/M phase arrest, and apoptosis of cancer cells. Furthermore, affinity-based fluorescence enhancement was observed during the binding of active compounds with tubulin, which greatly facilitated the determination of tubulin binding site of the compounds. Finally, selected compound **26** was found to exhibit obvious in vivo antitumor activity in A549 tumor xenografts model. Our systematic studies implied a new scaffold targeting tubulin and mitosis for novel antitumor drug discovery.



INTRODUCTION

Microtubules are ubiquitous slender filamentous dynamic polymers of α -tubulin and β -tubulin heterodimers in cell and serve as cell cytoskeleton for intracellular transports including movement of organelles, vesicles, proteins, or signaling molecules by motor proteins throughout the cell structure.¹ In the cell mitosis, highly dynamic microtubules also play a key role in completing the cell division by forming mitotic spindle, driving the intricate movement of chromosomes and separating sister chromatids.^{1a,2} Microtubule dynamics are tightly regulated both spatially and temporally.³ Tubulin binding molecules could induce abnormal mitotic spindles formation through interference with the dynamic instability of microtubules, thereby disrupting microtubules with the result of cell cycle arrest and apoptotic cell death.⁴

To date, microtubule dynamics has become one of the most successful anticancer targets.⁵ Many natural occurring and synthetic compounds interfering with microtubule dynamics have been developed. Paclitaxel, vinblastine, and colchicine represent the well-known three types of microtubule targeting agents which are distinct from their different binding domains named taxane, vinca, and colchicine binding site of β -tubulin, respectively.⁶ The vinca alkaloids⁷ and taxanes,⁸ identified respectively over 50 and 40 years ago, are currently administered in broad clinical indications.⁹ Recently, colchicine domain binding combretastatin A-4P (CA4P) as vascular disrupting agents has been approved for clinical trials.¹⁰ The mentioned representative drugs are shown in Figure 1. However, besides the rare resource and complex and expensive syntheses of some natural drugs like paclitaxel, many clinically applied microtubule targeting drugs easily acquire tumor

resistance and normally exhibit systematic toxicity, etc., which limited their clinical applications¹¹ and thus urged the prompted development of novel microtubule targeting agents for cancer treatment.

The natural occurring curcumin (1,7-bis(4-hydroxy-3-methoxyphenyl)-1,6-heptadiene-3,5-dione), a dietary yellow spice and pigment isolated from the rhizome of *Curcuma longa*, has been found to exhibit a wide range of biological activities, including anticancer, antimicrobial, anti-inflammatory, and antioxidation activities.¹² The promising biological profile and easy synthetic accessibility have triggered design and development of new curcumin derivatives as potential chemotherapeutic agents.^{12,13} In our previous studies, we reported a series of 4-arylidene curcumin analogues that could target nuclear factor κ B (NF- κ B) activation pathway with much enhanced cytotoxic activity than curcumin.¹⁴ During the structure optimization, meta-phenyl substituted chalcones (Figure 1) were proposed by structure moiety deletion and conformation restriction based on the preliminary analysis of the interaction of 4-arylidene curcumin with IKK β , in order to obtain improved potency in cytotoxicity. Biological evaluation revealed that most of these compounds showed moderate cytotoxic and NF- κ B inhibitory activity.¹⁵ Here we describe the design and biological evaluation of a series of ortho-aryl substituted chalcones (Figure 1) as extended efforts. Though demonstrated nonactive on NF- κ B inhibition, many of these new types of chalcones showed unexpectedly higher cytotoxicity than our previous reported 4-arylidene curcumins and

Received: January 6, 2014

Published: July 25, 2014

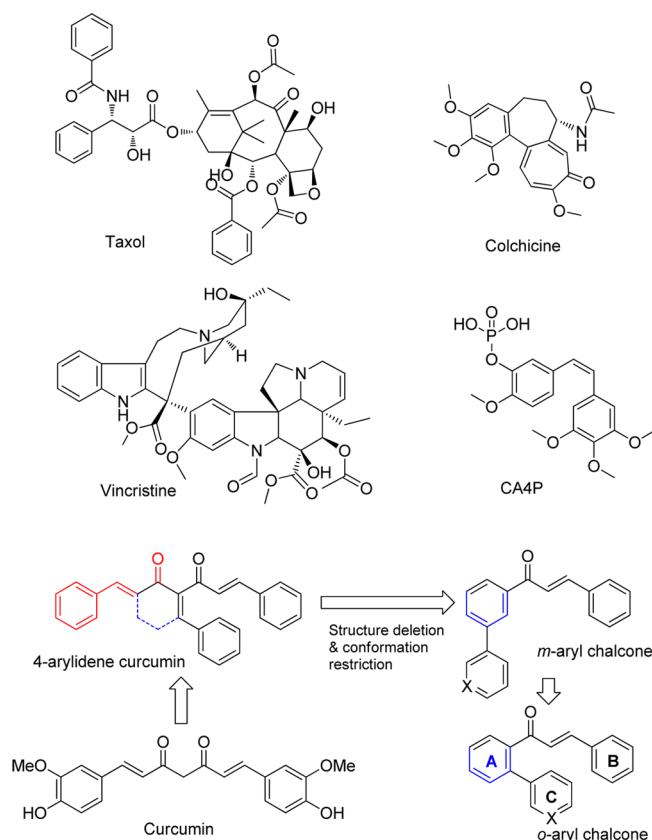


Figure 1. Structures of well-known microtubule-targeting agents and the design of aryl chalcones.

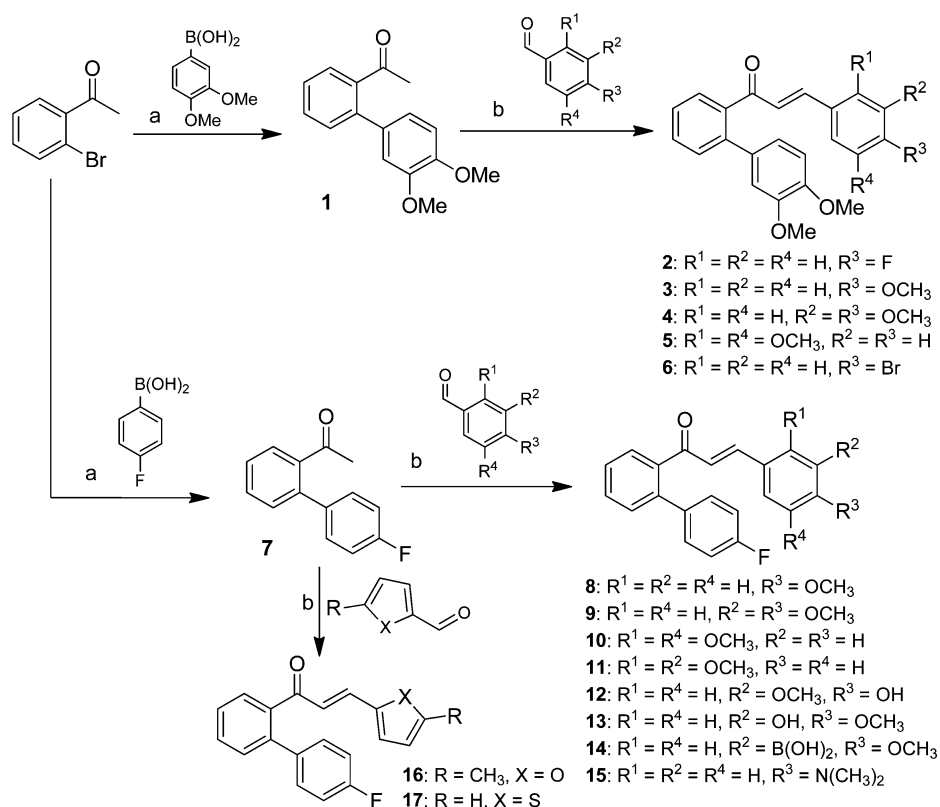
meta-phenyl chalcones, with IC_{50} values ranged from moderate to low nanomolar concentrations against a panel of parental and drug resistant cancer cell lines. The selected potent compounds are significantly superior to colchicine, paclitaxel (Taxol), doxorubicin, and vincristine in the growth inhibition of several drug resistant cancer cell lines, and furthermore, tubulin was identified as their potential molecular target by biological evaluations coupled with fluorescent assay based on the interesting affinity-induced fluorescent property of selected compounds. Finally, selected compound with high potency was found to exhibit obvious antitumor activity *in vivo*.

RESULTS AND DISCUSSION

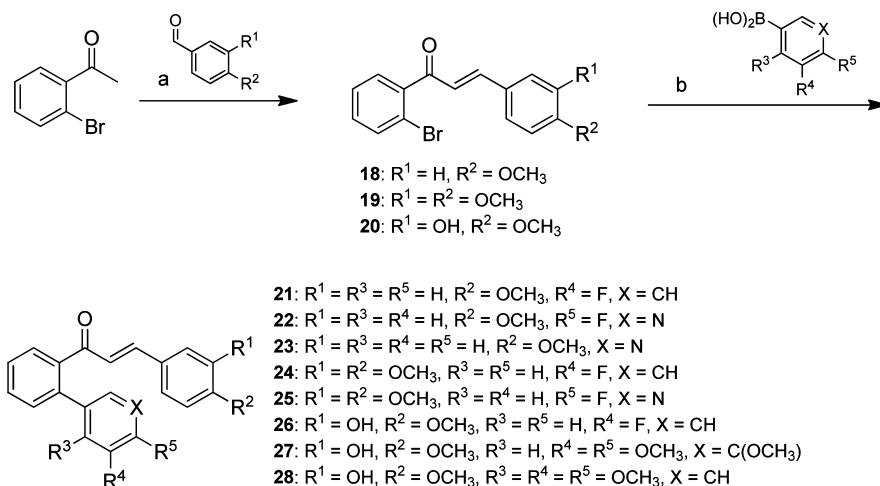
Chemistry. The ortho-aryl substituted chalcone analogues 2–6, 8–17 were synthesized as illustrated in Scheme 1. In brief, microwave assistant Suzuki coupling of 1-(2-bromophenyl)ethanone with (3,4-dimethoxyphenyl)boronic acid or (4-fluorophenyl)boronic acid yields biphenyl intermediate 1 or 7, respectively, and then KOH catalyzed aldol condensation of 1 or 7 with various arylaldehydes affords 2–6 or 8–17, respectively.

For the synthesis of 21–28, an aldol condensation followed by Suzuki coupling procedure was adopted. As illustrated in Scheme 2, chalcone intermediates 18–20 were prepared first by NaOH catalyzed aldol condensation and then coupled with various arylboronic acids by microwave assisted Suzuki reaction to give final products 21–28, respectively. Similar procedures were also used in the synthesis of analogues bearing reversed α,β -unsaturated ketone moiety (35–45) (Scheme 3).

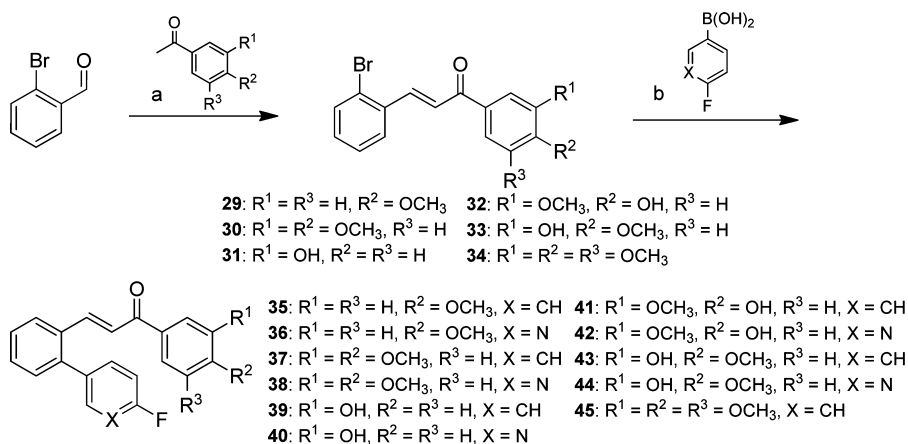
Scheme 1. Synthesis of Compounds 2–6 and 8–17^a



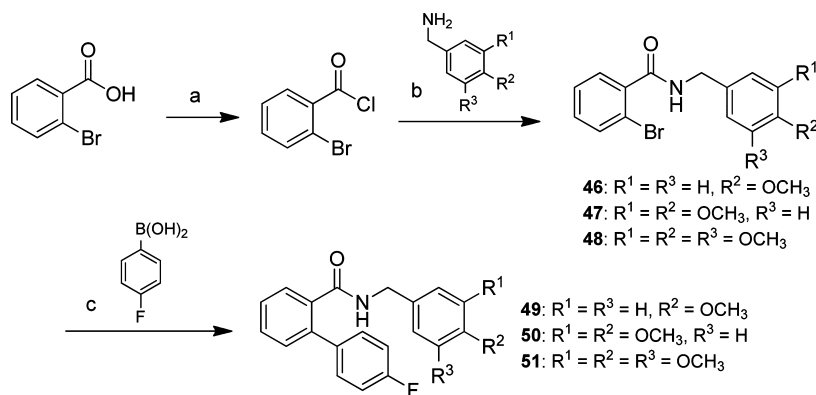
^aReagents and conditions: (a) $PdCl_2(dppf)$, 2 M K_2CO_3 , dioxane, microwave heating, 150 °C, 20 min; (b) KOH, EtOH, rt.

Scheme 2. Synthesis of Compounds 21–28^a

^aReagents and conditions: (a) 6 M NaOH (aq), EtOH, rt; (b) PdCl₂(dppf), 2 M K₂CO₃, dioxane, microwave heating, 150 °C, 20 min.

Scheme 3. Synthesis of Compounds 35–45^a

^aReagents and conditions: (a) 6 M NaOH (aq), EtOH, rt; (b) PdCl₂(dppf), 2 M K₂CO₃, dioxane, microwave heating, 150 °C, 20 min.

Scheme 4. Synthesis of Compounds 49–51^a

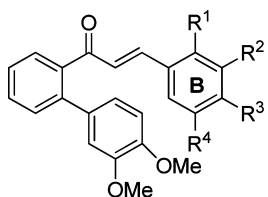
^aReagents and conditions: (a) SOCl₂, reflux; (b) toluene, TEA, reflux; (c) PdCl₂(dppf), 2 M K₂CO₃, dioxane, microwave heating, 150 °C, 20 min.

Preparation of 49–51 was achieved respectively by acylation of the different substituted benzylamine with 2-bromobenzoyl chloride to afford 46–48 first, followed by Suzuki coupling with 4-fluorophenylboronic acid, as shown in Scheme 4.

Antiproliferative Activity Evaluation of Obtained Compounds against a Panel of Cancer Cell Lines. To

evaluate the antiproliferative activity of obtained compounds, sulforhodamine B (SRB) assay was performed. Human lung carcinoma cell line A549, nasopharyngeal carcinoma cell line CNE2, colon carcinoma cell line SW480, breast carcinoma cell line MCF7, and hepatoma carcinoma cell line HepG2 were chosen. In actual work, the design of these compounds was

Table 1. Antiproliferative Activities of 2–6 against Different Cancer Cells

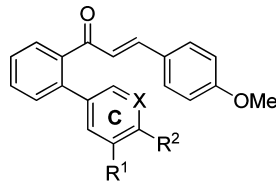


	R ¹	R ²	R ³	R ⁴
2	H	H	F	H
3	H	H	OCH ₃	H
4	H	OCH ₃	OCH ₃	H
5	OCH ₃	H	H	OCH ₃
6	H	H	Br	H

compd	IC ₅₀ ^a mean ± SE (μM)				
	A549	CNE2	SW480	MCF-7	HepG2
2	8.6 ± 1.4	5.4 ± 0.1	6.8 ± 0.6	7.1 ± 0.1	4.3 ± 0.3
3	1.6 ± 0.1	0.32 ± 0.02	0.89 ± 0.21	1.1 ± 0.0	0.60 ± 0.16
4	8.5 ± 1.4	2.5 ± 0.25	7.6 ± 0.6	4.9 ± 0.9	3.2 ± 0.5
5	4.1 ± 0.7	2.4 ± 0.5	5.2 ± 0.2	3.1 ± 0.4	2.1 ± 0.3
6	6.8 ± 0.9	4.8 ± 0.8	6.5 ± 0.2	8.3 ± 0.0	3.3 ± 1.6

^aData are presented as the mean ± SE from the dose–response curves of at least two independent experiments.

Table 2. Antiproliferative Activities of 8 and 21–23 against Different Cancer Cells

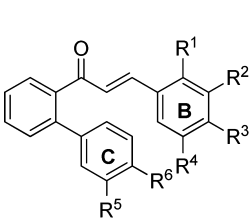
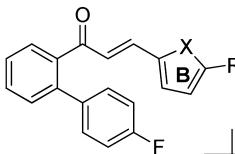


	R ¹	R ²	X
8	H	F	CH
21	F	H	CH
22	H	F	N
23	H	H	N

compd	IC ₅₀ ^a mean ± SE (μM)				
	A549	CNE2	SW480	MCF-7	HepG2
8	0.14 ± 0.04	0.053 ± 0.008	0.061 ± 0.008	0.67 ± 0.36	0.093 ± 0.023
21	0.28 ± 0.00	0.073 ± 0.001	0.14 ± 0.02	0.64 ± 0.35	0.11 ± 0.02
22	0.93 ± 0.03	0.16 ± 0.01	0.33 ± 0.04	2.7 ± 0.0	0.29 ± 0.02
23	0.58 ± 0.17	0.064 ± 0.007	0.20 ± 0.04	0.83 ± 0.28	0.097 ± 0.027

^aData are presented as the mean ± SE from the dose–response curves of at least two independent experiments.

Table 3. Antiproliferative Activities of 9–17, 24, and 26 against Different Cancer Cells

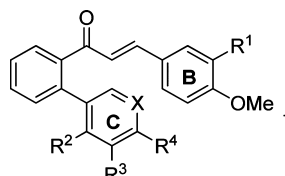
	R ¹	R ²	R ³	R ⁴	R ⁵	R ⁶
9	H	OCH ₃	OCH ₃	H	H	F
10	OCH ₃	H	H	OCH ₃	H	F
11	OCH ₃	OCH ₃	H	H	H	F
12	H	OCH ₃	OH	H	H	F
13	H	OH	OCH ₃	H	H	F
14	H	B(OH) ₂	OCH ₃	H	H	F
15	H	H	N(CH ₃) ₂	H	H	F
24	H	OCH ₃	OCH ₃	H	F	H
26	H	OH	OCH ₃	H	F	H

	R	X
16	CH ₃	O
17	H	S

compd	IC ₅₀ ^a mean ± SE (μM)				
	A549	CNE2	SW480	MCF-7	HepG2
9	0.44 ± 0.11	0.081 ± 0.008	0.57 ± 0.20	0.24 ± 0.05	0.095 ± 0.028
10	1.1 ± 0.2	0.75 ± 0.24	2.4 ± 0.1	1.7 ± 0.5	0.52 ± 0.18
11	7.1 ± 1.3	5.2 ± 0.5	5.7 ± 0.1	5.3 ± 0.9	5.0 ± 1.4
12	7.6 ± 2.1	2.5 ± 0.1	6.6 ± 0.6	4.0 ± 1.0	2.8 ± 0.2
13	0.065 ± 0.035	0.087 ± 0.010	0.057 ± 0.010	0.19 ± 0.08	0.023 ± 0.007
14	0.082 ± 0.013	0.021 ± 0.000	0.041 ± 0.009	0.22 ± 0.03	0.030 ± 0.003
15	0.073 ± 0.010	0.030 ± 0.002	0.041 ± 0.010	0.23 ± 0.06	0.047 ± 0.011
16	31 ± 1	14 ± 2	23 ± 0	23 ± 6	12 ± 2
17	12 ± 2	5.9 ± 0.8	16 ± 1	9.5 ± 1.7	6.2 ± 1.5
24	0.33 ± 0.04	0.65 ± 0.58	0.16 ± 0.02	1.2 ± 0.1	0.15 ± 0.01
26	0.011 ± 0.002	0.017 ± 0.004	0.010 ± 0.004	0.065 ± 0.020	0.0080 ± 0.0010
colchicine	0.050 ± 0.032	0.034 ± 0.005	0.033 ± 0.005	0.16 ± 0.09	0.035 ± 0.008
paclitaxel	0.0050 ± 0.0010	0.0030 ± 0.0003	0.0070 ± 0.0004	0.023 ± 0.004	0.028 ± 0.007

^aData are presented as the mean ± SE from the dose–response curves of at least two independent experiments.

Table 4. Antiproliferative Activities of 25, 27, and 28 against Different Cancer Cells

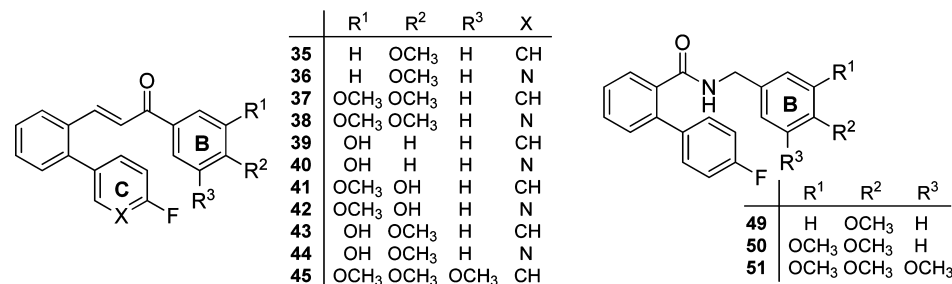


	R ¹	R ²	R ³	R ⁴	X
25	OCH ₃	H	H	F	N
27	OH	H	OCH ₃	OCH ₃	C(OCH ₃)
28	OH	OCH ₃	OCH ₃	OCH ₃	CH

compd	IC ₅₀ ^a mean ± SE (μM)				
	A549	CNE2	SW480	MCF-7	HepG2
25	1.2 ± 0.1	1.6 ± 0.9	1.3 ± 0.2	2.8 ± 0.5	1.0 ± 0.3
27	0.29 ± 0.00	0.79 ± 0.16	0.30 ± 0.05	0.68 ± 0.16	0.19 ± 0.02
28	0.19 ± 0.06	0.16 ± 0.06	0.17 ± 0.03	0.48 ± 0.06	0.23 ± 0.03

^aData are presented as the mean ± SE from the dose–response curves of at least two independent experiments.

Table 5. Antiproliferative Activities of 35–45 and 49–51 against Different Cancer Cells



	R ¹	R ²	R ³	X
35	H	OCH ₃	H	CH
36	H	OCH ₃	H	N
37	OCH ₃	OCH ₃	H	CH
38	OCH ₃	OCH ₃	H	N
39	OH	H	H	CH
40	OH	H	H	N
41	OCH ₃	OH	H	CH
42	OCH ₃	OH	H	N
43	OH	OCH ₃	H	CH
44	OH	OCH ₃	H	N
45	OCH ₃	OCH ₃	OCH ₃	CH

	R ¹	R ²	R ³
49	H	OCH ₃	H
50	OCH ₃	OCH ₃	H
51	OCH ₃	OCH ₃	OCH ₃

compd	IC ₅₀ ^a mean ± SE (μM)				
	A549	CNE2	SW480	MCF-7	HepG2
35	8.2 ± 2.0	9.0 ± 3.0	8.4 ± 1.5	8.8 ± 2.2	6.3 ± 1.1
36	>50	13 ± 7	10 ± 1	13 ± 3	8.2 ± 0.9
37	7.5 ± 0.6	7.6 ± 1.9	8.3 ± 0.5	7.1 ± 1.2	6.6 ± 0.7
38	17 ± 5	17 ± 5	15 ± 1	41 ± 2	17 ± 1
39	6.9 ± 1.3	7.3 ± 2.1	8.7 ± 0.1	9.3 ± 0.0	4.2 ± 0.1
40	6.9 ± 2.6	8.7 ± 3.5	7.4 ± 0.9	12 ± 2	6.4 ± 1.3
41	4.6 ± 1.3	4.8 ± 1.1	4.2 ± 0.4	5.4 ± 0.2	3.1 ± 0.1
42	13 ± 7	19 ± 9	8.5 ± 3.4	27 ± 1	9.9 ± 0.3
43	0.94 ± 0.64	0.75 ± 0.53	0.34 ± 0.15	0.56 ± 0.06	0.19 ± 0.01
44	3.2 ± 1.4	2.1 ± 1.3	1.6 ± 0.3	2.0 ± 0.7	1.8 ± 0.6
45	2.2 ± 0.3	3.8 ± 0.5	2.2 ± 0.0	9.1 ± 0.2	12 ± 2
49	>50	>50	>50	>50	>50
50	>50	>50	>50	>50	>50
51	>50	>50	>50	>50	>50

^aData are presented as the mean ± SE from the dose–response curves of at least two independent experiments.

based on an activity-guided approach. First, analogues 2–6 with the 3,4-dimethoxyl substituted on ring C (rings A, B, and C are defined in Figure 1 for convenience) were designed and evaluated, and the results in Table 1 indicate that compound 3 which bears a 4-methoxyl substitution on ring B increases the activity compared to the 3,4-dimethoxyl (4), 2,5-dimethoxyl (5), or 4-halogen (F or Br, 2 and 6) substitutions, showing low micromolar concentration of IC₅₀ value against the five tested cancer cell lines (IC₅₀ of 0.32–1.6 μM).

This result leads to the design and evaluation of more analogues with different substituted phenyl or pyridinyl of ring C and the same 4-methoxyl substitution on ring B (8, 21–23). The data summarized in Table 2 show that all of the four compounds generally exhibit higher cytotoxicity than 3, with submicromolar concentration of IC₅₀ (0.053–0.93 μM) except for the individual case of 22 against the MCF-7 cell line (IC₅₀

of 2.7 μM), and the fluoro-substituted analogue 8 is demonstrated to be the most potent of these derivatives.

From Table 2, we also learned that the replacement of phenyl with pyridinyl at position of ring C decreased slightly the cytotoxicity in general. Therefore, 3- or 4-fluoro substituted phenyl of ring C was reserved and the moiety of ring B was redesigned for evaluation. The inhibitory effects of the resulting 24, 26, and 9–17 were summarized in Table 3. Among the analogues with 4-F substitution, compounds with 3,4-dimethoxyl and 2,5-dimethoxyl on ring B (9 and 10, respectively) exhibit generally lower activity (IC₅₀ of 0.081–2.4 μM) than 8 (IC₅₀ of 0.053–0.67 μM), which is in consistence with the rule revealed by comparing 3 with 4 and 5. Meanwhile, 2,3-dimethoxyl (11) and 4-hydroxyl-3-methoxyl (12) substitutions on ring B further decrease the activities (IC₅₀ of 2.5–7.6 μM) than 9 and 10; all of the above information indicated that the methoxyl substitutions in the meta or ortho

Table 6. Drug Tolerances of Selected Compounds against Different Drug Resistant Cancer Cells

compd	IC ₅₀ ^a mean ± SE (μM)									
	A2780	A2780/TAX	DRI ^b	HCT-8	HCT-8/VCT	DRI	A549/CDDP	DRI	MCF-7/DOX	DRI
8	0.17 ± 0.01	0.69 ± 0.00	4.1	0.22 ± 0.05	0.23 ± 0.02	1.0	0.21 ± 0.06	1.1	0.12 ± 0.17	0.29
13	0.027 ± 0.009	0.50 ± 0.01	18	0.038 ± 0.020	0.42 ± 0.03	11	0.43 ± 0.22	10	0.0070 ± 0.0003	0.040
14	0.063 ± 0.015	0.23 ± 0.06	3.6	0.063 ± 0.009	0.084 ± 0.015	1.3	0.074 ± 0.004	1.1	0.024 ± 0.001	0.60
15	0.094 ± 0.020	0.049 ± 0.012	0.52	0.13 ± 0.02	0.096 ± 0.009	0.72	0.11 ± 0.04	1.6	0.045 ± 0.007	0.68
21	0.16 ± 0.01	0.86 ± 0.12	5.2	0.20 ± 0.02	0.22 ± 0.00	1.1	0.48 ± 0.16	2.1	0.084 ± 0.012	0.64
26	0.013 ± 0.005	0.23 ± 0.01	18	0.016 ± 0.008	0.057 ± 0.015	3.6	0.18 ± 0.11	16	0.0020 ± 0.0003	0.030
27	0.38 ± 0.17	1.6 ± 0.2	4.3	0.52 ± 0.26	2.0 ± 0.1	4.0	0.59 ± 0.19	2.0	0.17 ± 0.03	0.24
COL	0.057 ± 0.003	0.59 ± 0.08	10	0.059 ± 0.007	1.1 ± 0.4	19	0.081 ± 0.011	2.3	3.2 ± 0.2	169
TAX	0.015 ± 0.009	2.9 ± 0.5	196	0.021 ± 0.013	2.6 ± 0.9	124	0.0090 ± 0.0020	1.8	7.6 ± 1.0	2525
DOX	ND ^c	1.9 ± 0.3	ND ^c	ND ^c	3.4 ± 0.3	ND ^c	0.29 ± 0.02	1.0	15 ± 4	106
VCT	ND ^c	0.93 ± 0.05	ND ^c	ND ^c	1.9 ± 0.5	ND ^c	0.056 ± 0.017	4.7	4.3 ± 0.8	1063

^aData are presented as the mean ± SE from the dose–response curves of at least two independent experiments. A2780 and HCT-8 were also evaluated as the parental control cells in this assay. ^bDrug resistant index: (IC₅₀ of drug resistant cancer cell)/(IC₅₀ of parental cancer cell). ^cND = not determined.

position of the ethylenic linkage of ring B contribute negatively to the activities. On the other hand, replacements of ring B by heterocyclic furan (**16**) or thiophen (**17**) moiety largely decreased their activity (IC₅₀: of 5.9–31 μM).

Interestingly, compared to **8**, a further substitution of 3-hydroxyl (**13**), 3-boric acid (**14**), or replacement of 4-methoxyl with 4-*N,N*-dimethyl (**15**) on ring B dramatically increased the activities, and IC₅₀ values closer or comparable to those of colchicine (IC₅₀ of 0.033–0.16 μM) and paclitaxel (IC₅₀ of 0.0030–0.028 μM) were observed. Except for the inhibition of MCF-7 (IC₅₀ of 0.19–0.23 μM), all three compounds show IC₅₀ values in nanomolar concentration range (0.021–0.087 μM) on the other four cancer cell lines. At the same time, compound **26**, which was structurally different from **13** by the position of fluoro substitution on ring C, generally demonstrated the highest inhibitory activity (IC₅₀ of 0.0080–0.065 μM), shows superior potency to the colchicine, and is less potent in 4/5 cell lines but in one case (HepG2) has higher potency than paclitaxel. Methylation of the 3-hydroxyl on ring B of **26** yields much less active compound **24** (IC₅₀ of 0.15–1.2 μM), which is consistent with the above conclusion that methoxyl substitutions on ring B in the meta position of the ethylenic linkage greatly decrease the activity.

More structure–activity relationship information was therefore investigated. **25**, the pyridinyl containing compound, exhibits obvious lower activity than **9**, suggesting again that the pyridine moiety on ring C does not favor the activity (Table 4). Noticeably, trimethoxyl substituted phenyl moiety frequently appeared in highly active tubulin binders such as colchicine, CA4P, and many of their derivatives and mimics. We found that the incorporated compounds **27** and **28** (IC₅₀ of 0.16–0.79 μM) display much lower activity than **13** and **26**, respectively, though with submicromolar concentration of IC₅₀ (Table 4).

To probe the contribution of the α,β-unsaturated ketone moiety to the cytotoxicity, analogues with directional reversed α,β-unsaturated ketone moiety **35–45** and replacements of amide moiety (**49–51**) were examined. The results were summarized in Table 5. We found that **35–45** only show low to moderate inhibitory activity against the tested five cancer cell lines except the 3-hydroxyl-4-methoxyl substitution bearing compound **43**. Meanwhile, no obvious cytotoxicity was observed on **49–51** at concentrations up to 50 μM. By further comparing the activity of **8** vs **35** and **49**, **9** vs **37** and **50**, **12** vs

41, and **22** vs **36**, we concluded that the α,β-unsaturated ketone moiety itself and its direction in the molecular scaffold were crucial for their cytotoxicity.

A main drawback of clinically used anticancer drugs is the drug resistance of tumor cells. Therefore, we also evaluate the antiproliferation activities of selected compounds against a panel of parental and drug resistant cancer cell lines to demonstrate their potential in anticancer. We chose the representative and commercially available human ovarian carcinoma cell A2780 with the paclitaxel resistant cell A2780/TAX and human ileocecum carcinoma cell HCT-8 with the vincristine resistant cell HCT-8/VCT as the paclitaxel and vincristine resistant models, respectively. Furthermore, the cisplatin resistant cell A549/CDDP and doxorubicin resistant cell MCF-7/DOX were chosen as representative models for well-known multidrug resistant cancer cells. Highly active compounds **13–15** and **26** with relative less active compounds **8**, **21**, and **27** were selected for the examination. Colchicine, paclitaxel, vincristine, and doxorubicin were employed as positive controls. The results were summarized in Table 6.

The results show that the drug resistance of MCF-7/DOX was overcome by all selected compounds **8**, **13–15**, **21**, **26**, and **27** with significantly lower IC₅₀ value than that against MCF-7. The drug resistant index (DRI), which were calculated from the ratio of IC₅₀ from drug resistant cancer cell over the IC₅₀ from parental cancer cell (Table 6), ranged from 0.03 to 0.68, and most active compounds **13** (IC₅₀ = 0.0070 μM) and **26** (IC₅₀ = 0.0020 μM) show dramatically high potency in the MCF-7/DOX growth inhibition; similar results were observed in the cases of **15** against A2780/TAX (IC₅₀ = 0.049 μM, DRI = 0.52) and HCT-8/VCT (IC₅₀ = 0.096 μM, DRI = 0.72). No obvious drug tolerance was found (DRI < 1.5) in the cases of **8** and **14** against HCT-8/VCT and A549/CDDP and of **21** against HCT-8/VCT. Slight to moderate drug resistance was observed in the cases of **8**, **13**, **14**, **21**, **26**, **27** against A2780/TAX (DRI = 3.6–18), **13**, **26**, **27** against HCT-8/VCT (DRI = 3.6–11), and **13**, **15**, **21**, **26**, **27** against A549/CDDP (DRI = 1.6–16). Nevertheless, all these compounds exhibit inhibitory effects against the tested cancer cell lines with submicromolar concentration of IC₅₀ except for the individual case of **27**.

Noticeably, though the positive controls colchicine, paclitaxel, vincristine, and doxorubicin show high activity in all tested parental cancer cell lines, all of them were greatly tolerated by the tested drug resistant cancer cell lines A2780/TAX (DRI =

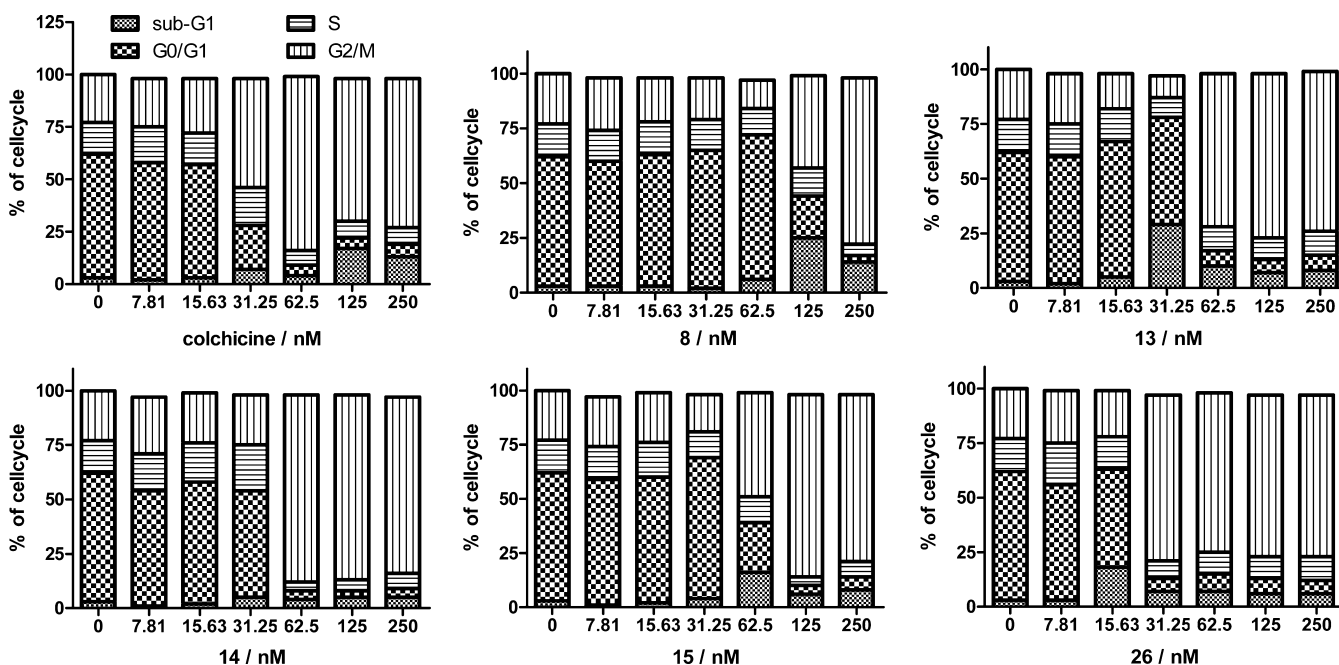


Figure 2. Cell cycle distribution of A549 with or without treatment of different compounds. A549 cells were plated in 96-well plates for 24 h and treated without and with different concentrations of tested compounds 8, 13, 14, 15, and 26 (0, 7.81, 15.63, 31.25, 62.5, 125, and 250 μM), and colchicine treated with the same concentration as the control. After 24 h, cells were fixed by 4% paraformaldehyde and stained by Hoechst 33342 and then analyzed by ArrayScan VTI high content analysis system.

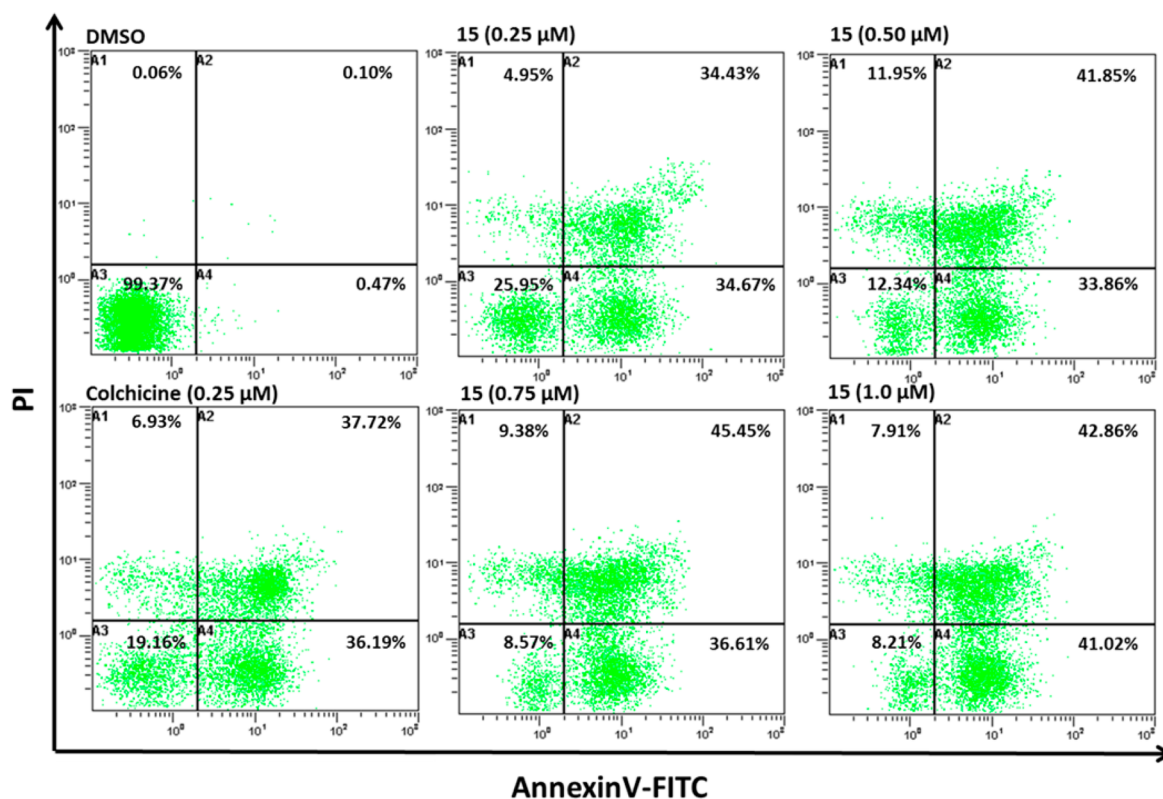


Figure 3. 15 induced apoptosis of A549 cells. Cells were seeded in a six-well plate for 24 h. Then different concentrations of 15 (0.25, 0.50, 0.75, and 1.0 μM) and positive control colchicine (0.25 μM) were added for 48 h. Then 1×10^5 cells were collected by centrifugation and resuspended in 500 μL of $1 \times$ binding buffer and were analyzed by flow cytometer after being stained by 5 μL of annexin V-FITC and 10 μL of propidium iodide for 5 min in the dark.

10–196), HCT-8/VCT (DRI = 19–124), and MCF-7/DOX (DRI = 106–2525) and slightly resisted by A549/CDDP (DRI = 1.8–4.7) except for doxorubicin. Furthermore, the IC_{50}

values of positive controls are significantly higher than those of 13–15 and 26 by several to thousands times during the growth inhibition of A2780/TAX, HCT-8/VCT, and MCF-7/

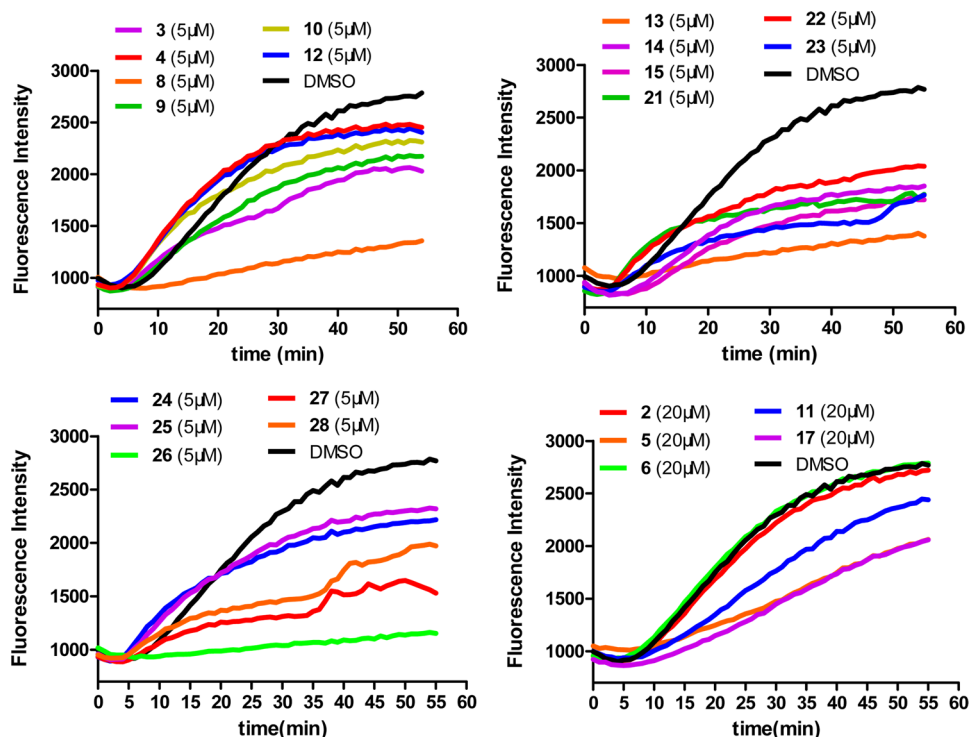


Figure 4. Effects of selected compounds on the microtubule polymerization. Tubulin was mixed with selected compounds in general tubulin buffer containing 1 mM GTP and 20% glycerol. Microtubule polymerization was monitored in kinetic model of FlexStation 3 multimode reader (excitation, 360 nm; emission, 450 nm).

DOX. To explore the potential mechanism under the observation, we examined the intracellular P-gp function by rho123 accumulation and efflux assay in A2780/TAX, HCT-8/VCT, and MCF-7/DOX and their parental cell lines. We found that rho123 accumulated very well in all three parental cell lines, and no obvious efflux was observed during the examined time (Supporting Information, Figures S1 and S2d). On the contrary, much lower rho123 accumulation was observed in three drug resistant cancer cells and the accumulated rho123 obviously eliminated along with the time consumption (Supporting Information, Figures S1 and S2a–c). These results indicated a much elevated intracellular P-glycoprotein function in the investigated three drug resistant cancer cell lines. Reasonably, our compounds may evade a drug efflux pump mechanism which may affect the positive control drugs such as paclitaxel, doxorubicin, and vincristine.

Taking the above results together, we discovered that 3'- or 4'-fluoro substituted 1-([1,1'-biphenyl]-2-yl)-3-phenylprop-2-en-1-one may serve as potent cytotoxic scaffold, especially with 3-hydroxyl-4-methoxyl, 3-boric acid 4-methoxyl, or 4-*N,N*-dimethyl substituted on ring B.

Active Analogues Induce G2/M Arrest and Apoptosis of A549 Cells. As we mentioned before, the aryl-substituted chalcones were originally designed to improve the potency to inhibit the NF- κ B activation pathway.¹⁵ Unfortunately, we found that the *o*-aryl chalcones totally lost their ability of NF- κ B blockage (data not shown). However, the finding of highly active compounds encouraged us to search for their potential molecular target. Therefore, we first investigated the effects of the found active compounds on the cell cycle. 8, 13–15, and 26 were chosen and evaluated on the A549 cancer cell line. A549 was treated with different concentrations of employed compounds for 24 h. The nuclei were stained with Hoechst

33342, and the fluorescence was recorded by ArrayScanVTI high content analysis system. The percentage of each cell cycle phase was calculated by the ratio of the population of cells with certain gated fluorescence intensity over the total counted cell number. The results are shown in Figure 2. An obvious G2/M phase arrest is observed in all 8, 13–15, and 26 treated A549 cells, which are similar to the positive control colchicine. Colchicine induces significant G2/M arrest at 31.25 nM concentration, the same as 26 achieved. 13–15 induced obvious G2/M arrest at 62.5 nM, and the less active function of 8 was observed at 125 nM.

To assess whether the active compound would induce cancer cell apoptosis, 15 treated A549 cells were stained with annexin V-FITC and propidium iodide (PI) and analyzed. The flow cytometric data (Figure 3) show concentration-dependent high activity on stimulating cell apoptosis, and the total numbers of early and late apoptotic cells were 69.10%, 75.71%, 82.06%, and 83.88% in the cases of 0.25, 0.50, 0.75, and 1.0 μ M 15 treated A549 cells, respectively. Positive control colchicine (0.25 μ M) induced 36.19% and 37.72% early and late apoptosis cells, respectively. In contrast, only 0.47% and 0.10% early and late apoptotic cells were found in untreated control. This result confirmed that 15 could induce efficient apoptosis of A549.

Microtubule Polymerization Inhibition of Selected Compounds. The above data suggest that these molecules may interfere with the mitotic phase and induce apoptosis of cancer cells, which are typical properties of microtubule binding agents.^{4c,16} Therefore, we evaluated the effects of different compounds on the polymerization of tubulin by using the colchicine as positive control. First, the employed compounds were evaluated at 5 or 20 μ M concentration (Figure 4). We found that compounds with at least three of IC₅₀ values below 1.0 μ M (3, 8, 9, 13–15, 21–23, and 26–28) against the first

Table 7. IC₅₀ of Selected Compounds on Inhibition of Tubulin Polymerization

	8	13	14	15	21	26	27	colchicine
IC ₅₀ ± SE (μM) ^a	1.8 ± 0.0	1.3 ± 0.0	3.4 ± 0.2	3.6 ± 0.0	4.0 ± 0.3	0.49 ± 0.27	2.8 ± 0.2	2.6 ± 0.6

^aIC₅₀ presented as mean ± SE from at least two independent experiments.

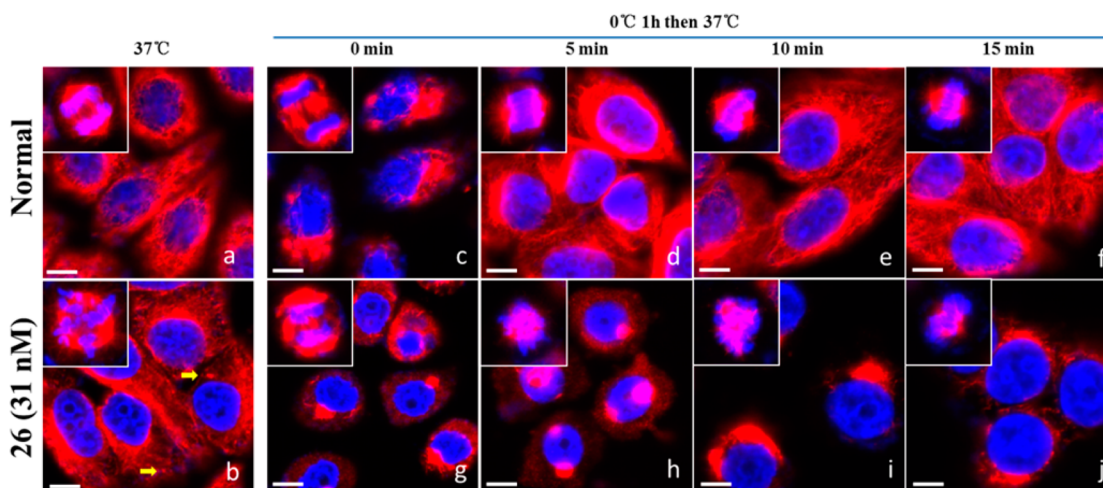


Figure 5. Effects of 26 on the cellular microtubule network and microtubule reassemble by immunofluorescence. Cells were incubated with 0.5% DMSO (a, c–f) or 31 nM 26 (b, g–j) at 37 °C for 24 h, and then direct microscopy detection (a, b) of the fixed and stained cell was performed. In the microtubule regrowth assay, cells were chilled on ice for 1 h first, then warm at 37 °C. Cells with 0 (c, g), 5 (d, h), 10 (e, i), and 15 min (f, j) warm-up time were fixed and stained and then recorded by confocal microscopy. Insets show the mitosis cell. The cellular microtubules were stained with primary β-tubulin mouse antibody and Dylight 549 goat anti-mouse IgG (red). DNA was stained by 4',6-diamidino-2-phenylindole (DAPI, blue). Scale bars: 10 μm.

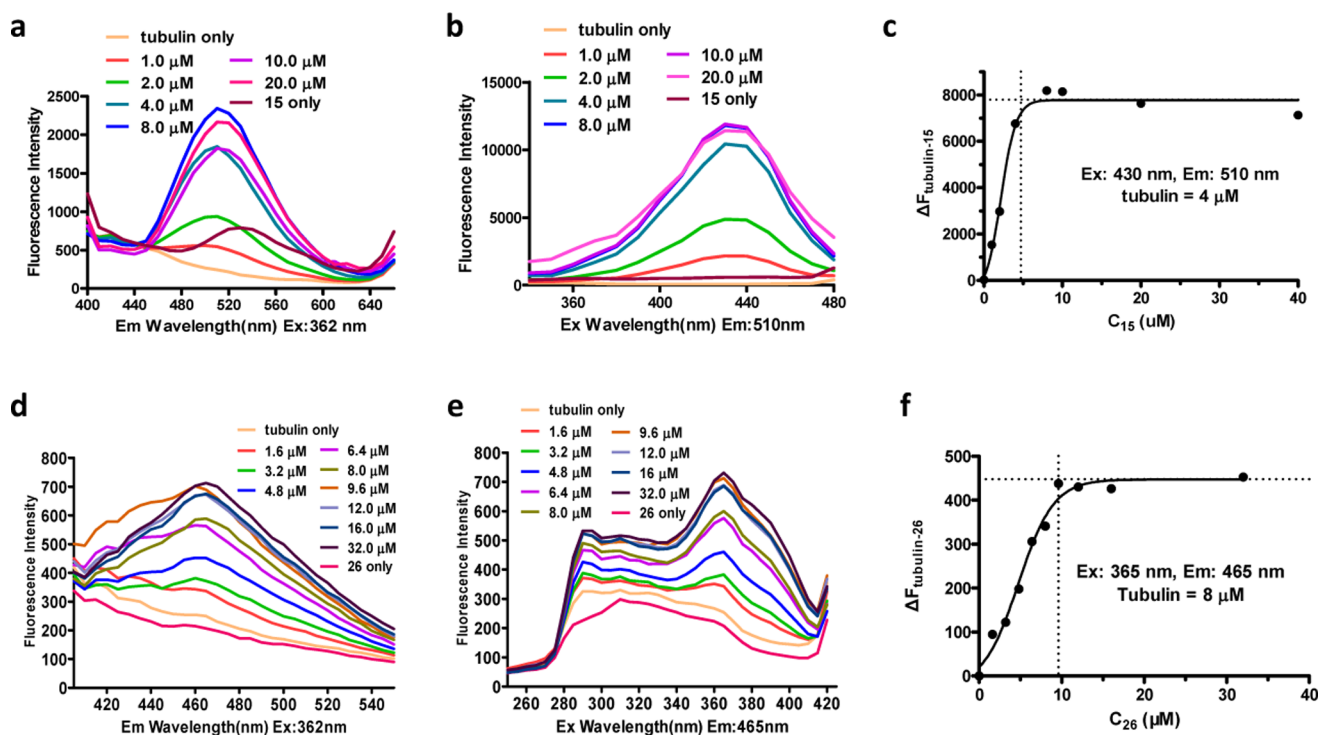


Figure 6. Affinity-induced fluorescence by the binding of 15 or 26 to tubulin. Various concentrations of 15 (a–c) or 26 (d–f) were mixed with or without 4 μM (15) and 8 μM (26) tubulin and incubated in general tubulin buffer for 30 min. Fluorescent emission spectrum of each compound was recorded under the optimal excitation wavelength of 362 nm (a, d) and at 510 nm (15, b) and 460 nm (26, e) emission wavelengths, respectively. The concentrations of both the tubulin- or compound-only control are 4 μM tubulin for 10 μM 15 binding and 8 μM tubulin for 8 μM 26 binding, respectively. (c) and (f) show that the enhanced fluorescence (ΔF), induced by various concentrations of 15 with 4 μM tubulin (c) or of 26 with 8 μM tubulin (f) at the optimal excitation and emission wavelengths, respectively, and calculated from the increments of stable fluorescence emission over the fluorescence intensity with tubulin only in each case, varied with the concentrations of compounds.

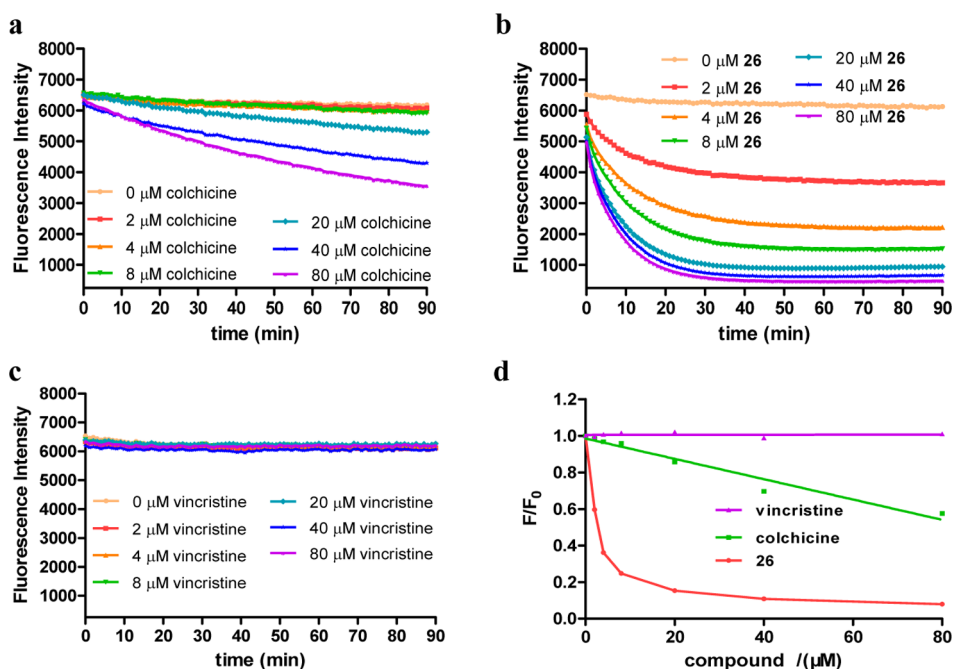


Figure 7. Competitive binding assay of colchicine, **26**, and vincristine with **15** in the presence of tubulin. $8 \mu\text{M}$ **15** and $4 \mu\text{M}$ tubulin were incubated until the fluorescence of tubulin–**15** complex reach a stable level. Time-course fluorescence was detected at 430 and 510 nm as excision and emission wavelengths, respectively, right after the addition of various concentrations of colchicine (a), **26** (b), and vincristine (c). The decreased stable fluorescence ratio of colchicine, **26**, and vincristine treated well (F) at each concentration to the original fluorescence intensity of **15**–tubulin (F_0) was plotted and fitted (d).

screened five cancer cell lines obviously inhibited the microtubule polymerization, and **8**, **13**, **26**, and **27** show the most potent activity. With the decrease of the cytotoxicity (**10** and **25**), the inhibitory activity toward microtubule polymerization reduced accordingly. As expected, no significant microtubule polymerization inhibition was observed after treatment with low cytotoxic compounds (**4**, **12** at $5 \mu\text{M}$ or **2**, **6** at $20 \mu\text{M}$) except for the moderate inhibition of **5**, **11**, and **17** at $20 \mu\text{M}$. This result suggested a general correlation between the cytotoxicity with the microtubule polymerization inhibitory activity.

Various concentrations of compounds with high cytotoxicity or microtubule polymerization inhibitory activity (**8**, **13**–**15**, **21**, **26**, **27**) were therefore examined, and the IC_{50} was calculated. The results (Table 7) indicate that **8** ($\text{IC}_{50} = 1.8 \mu\text{M}$), **13** ($\text{IC}_{50} = 1.3 \mu\text{M}$), and **26** ($\text{IC}_{50} = 0.49 \mu\text{M}$) exhibit stronger activity than colchicine ($\text{IC}_{50} = 2.6 \mu\text{M}$). This work revealed that these active cytotoxic molecules may target microtubule to exhibit cytotoxicity.

26 Inhibits Microtubule Reassemble and Leads to Multipolar Mitosis in Nanomolar Concentration. To further confirm the molecular target of the found cytotoxic compounds, we investigated the effects of **26** on the cellular microtubule network, reassembly of microtubule,¹⁷ and the mitosis in A549 cells by confocal microscopy (Figure 5). Normal filiform and meshy microtubule network and bipolar mitotic division were present in the DMSO treated cells (Figure 5a). In contrast, low concentration of **26** (31 nM) efficiently induced the disruption of microtubule network, resulting in massive and dotted microtubule disorder formation (Figure 5b, region pointed by yellow arrow), and the multipolarization of spindle and multinucleation phenomena were observed. In the microtubule regrowth assay, cold treatment of the cells almost completely depolymerized the

microtubule, and the obvious microtubule regrowth occurred along with the warm-up process. The microtubule network and normal cell mitosis recovered after a 15 min warmup (Figure 5c–f). Meanwhile, 31 nM **26** almost completely inhibited the reassembly of microtubule in both interphase and mitosis cells, accompanied by disorganized mitosis as indicated by the observed multipolarization of spindle and multinucleation phenomena (Figure 5g–j).

This result validated that **26** can inhibit microtubule organization and interfere the mitosis of A549 in much lower effective concentration than that to microtubule polymerization inhibition. These results implied that the microtubule dynamics is easier to be interfered by the microtubule targeting agents than the microtubule polymerization, which is consistent with the finding of many previous reports.¹⁸

15 and **26** Show Affinity-Based Fluorescence Enhancement during Binding to Tubulin. Interestingly, a fluorescent emission phenomenon was observed during the interaction of **15** or **26** with tubulin, respectively. At 362 nm excitation wavelength, $4 \mu\text{M}$ **15** showed slight fluorescent emission at 530 nm; however, in the presence of $4 \mu\text{M}$ tubulin, fluorescent emission appeared at 510 nm, with intensity increasing with the increasing concentration of **15** (Figure 6a). A similar phenomenon was also observed in the **26**–tubulin interaction. At 362 nm excitation wavelength, $8 \mu\text{M}$ **26** showed no fluorescent emission and in the presence of $8 \mu\text{M}$ tubulin, fluorescent emission appeared at 465 nm, which is concentration dependent (Figure 6d). Excitation wavelength scanning revealed that the fluorescence intensity increased with increasing concentration of **15** (Figure 6b) or **26** (Figure 6e) in the presence of tubulin, while tubulin or compound alone showed no obvious fluorescence upon the excitation of **15** and **26** at 430 and 365 nm, respectively, suggesting affinity-induced fluorescent properties observed in tubulin–**15** (or **26**) complex.

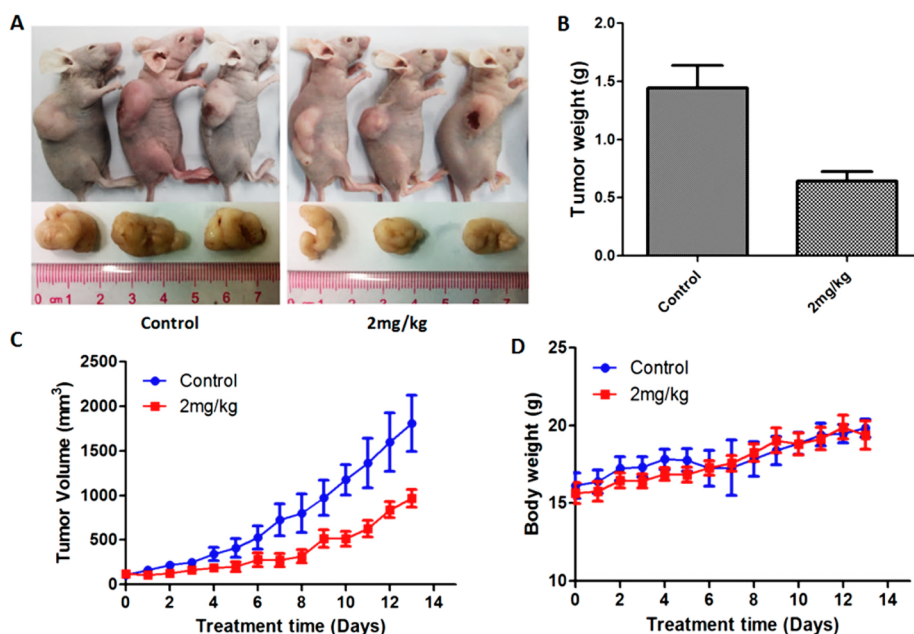


Figure 8. Antitumor activity of **26** toward A549 tumor xenografts.

Kinetic analysis was therefore carried out. Fluorescence intensity was recorded right after the mixing of various concentrations of **15** with $4 \mu\text{M}$ tubulin (excitation, 430 nm; emission, 510 nm) or **26** with $8 \mu\text{M}$ tubulin (excitation, 365 nm; emission, 465 nm), respectively. Fluorescence intensity of **15**–tubulin complex increased in a time dependent manner and finally reached a stable plateau in less than 30 min, while **26** induced fast fluorescence saturation after quickly mixing with tubulin (Supporting Information, Figure S3), indicating a rapid binding of **26** with tubulin. The stable fluorescence showed a dose dependent manner in both cases of **15** and **26**, and the time course of the fluorescence enhancements from **15**–tubulin (Figure 6c) or **26**–tubulin binding (Figure 6f) suggested that the fluorescence enhancements reached maximum when the concentration ratio of compound with tubulin is close to 1:1.

15 and 26 Binding to Colchicine Domain of Tubulin. It is well-known that colchicine also showed affinity-induced fluorescence enhancement (excitation, 362 nm; emission, 435 nm) with tubulin,¹⁹ which was widely used to determine whether other investigated compounds are binding to the colchicine site.²⁰ For the case of vincristine site binding, however, ³H labeled vincristine is usually needed.^{20,21} Fortunately, the interesting fluorescent properties of our compounds allow us to examine their binding site by fluorescent competitive assay. Owing to the overlay of the excitation and emission wavelength of **26** with colchicine, $8 \mu\text{M}$ **15** was chosen, which is incubated with tubulin ($4 \mu\text{M}$) until the fluorescence intensity reached the stable state after 30 min. Then various concentrations of colchicine, **26**, and vincristine were added, respectively, and the kinetic curves were recorded accordingly (Figure 7). Colchicine decreased the fluorescence of **15**–tubulin complex in a concentration dependent manner, indicating a competitive binding of **15** with colchicine in the same binding domain, and $20 \mu\text{M}$ colchicine efficiently replaced **15** from tubulin (Figure 7a and Figure 7d). Noticeably, **26** was more potent than colchicine. Addition low concentration to $2 \mu\text{M}$ **26** induced dramatic decrease of the fluorescence of **15**–tubulin complex, which reflected the higher affinity of **26** than that of colchicine (Figure 7b and Figure 7d) toward tubulin.

This result is consistent with the observed higher potency of **26** in cytotoxicity and tubulin polymerization than that of colchicine. In contrast, addition of vincristine would not affect the fluorescence of the **15**–tubulin complex, which excluded the possible binding of **15** in the vincristine domain (Figure 7c,d).

Interestingly, the employed aryl chalcones may also serve as Michael acceptors to biological nucleophiles, mostly attributed to the presence of an α,β -unsaturated ketone moiety, which is readily modified by the free thiol group in the protein structure.²² Accordingly, we found that preincubation of tubulin with the 5,5'-dithiobis(2-nitrobenzoic acid) (DTNB) disabled the affinity-induced fluorescence of **26**–tubulin complex dose-dependently (Supporting Information, Figure S4),^{20,23} which indicated that the thiol groups in tubulin may participate compound–tubulin binding. In antiproliferation assay, the α,β -unsaturated ketone moiety indeed was proved to be crucial to the cytotoxicity. IC_{50} values of compounds **49**–**51** were greater than $50 \mu\text{M}$. We therefore cannot exclude the possibility of a covalent modification of tubulin through these active compounds. In fluorescent competitive assay, however, the observation of **15** in tubulin replaced by colchicine and **26** suggested that these active aryl-substituted chalcones could reversibly bind to the colchicine site. From this point of view, the semirigid α,β -unsaturated ketone moiety may promote the binding by maintaining a favorable conformation of active aryl chalcones during the interaction, and in the cases of compounds **49**–**51**, the amide bonds are more elastic which may thus disrupt the favorable conformation. We unfortunately failed to obtain a proper binding pose of active compound in tubulin by molecular docking analysis upon the reversible binding model (data not shown). However, all of the above information may imply a more complicated situation of the investigated chalcone–tubulin interaction. Does a reversible covalent interaction exist during the colchicine site binding? The raised question may need systematic investigation in future work.

26 Inhibits A549 Tumor Xenografts Growth in Vivo. To evaluate the role of **26** in tumor proliferation in vivo, we

examined the ability of **26** to suppress the growth of A549 tumor xenografts in nude mice. Mice were treated with **26** every other day for 2 weeks. **26** significantly inhibits the growth of tumor xenografts (Figure 8A). The excised tumors from the control group weighed between 1.11 and 1.96 g (mean, 1.446 g), whereas those from the 2 mg/kg body weight **26**-treated animals ranged from 0.38 to 0.90 g (mean, 0.641 g) (Figure 8B). In addition, treatment with compound **26** at 2 mg/kg body weight resulted in a significant decrease in final tumor volume (mean, 965.6 mm³) when compared to the control group (mean, 1806.9 mm³; Figure 8C), while keeping a stable increase of mice body weights (Figure 8D). These data show that **26** has the ability to inhibit lung cancer growth in nude mice bearing A549 xenografts via proliferation suppression.

CONCLUSIONS

In summary, we designed and synthesized a series of substituted ortho-aryl-substituted chalcones, and potent cytotoxic agents were found with most IC₅₀ values at nanomolar concentration range against a panel of cancer cell lines. The active compounds such as **13–15** and **26** show superior potency by several to thousands times than those of paclitaxel, doxorubicin, colchicine, and vincristine in the growth inhibition of paclitaxel resistant A2780/TAX, vincristine resistant HCT-8/VCT, cis-platinum resistant A549/CDDP, and doxorubicin resistant MCF-7/DOX. The most potent compounds **13** and **26** show dramatic low IC₅₀ values of 7 and 2 nM, respectively, toward MCF-7/DOX. Furthermore, the in vivo antitumor potency of **26** were confirmed in A549 tumor xenografts model.

The cell cycle analysis, immunofluorescence visualization, and tubulin polymerization inhibition assay further confirmed that the selected active compounds could greatly inhibit in vitro and cellular tubulin polymerization, interfere with the mitosis, and thus lead to G2/M cell cycle arrest and apoptosis of the treated cancer cells. Interestingly, compounds **15** and **26** were found to exhibit affinity-induced fluorescence during the binding to tubulin. On the basis of this special optical characterization, we further found the active compounds may interact with β -tubulin in the colchicine binding site. Our finding revealed a new scaffold and opportunities for mitosis-targeting drug discovery.

EXPERIMENTAL SECTION

1. General. All commercial reagents and solvents were purchased from vendors and were used without further purification or distillation. Microwave reactions were performed in a Biotage Initiator 2.5 microwave reactor. The purities of compounds used for biological evaluation (>95%) were determined on a DIONEX Ultimate 3000 HPLC system (Chromleon SR9 Build 2673): column, Acclaim 120 C₁₈, 5 mm, 4.6 mm × 250 mm; flow rate, 1 mL/min. Samples were eluted with a gradient up to 95% solvent A over 30 min and detected at 254 nm, whereas the A is CH₃CN in double-deionized H₂O with 0.1% trifluoroacetic acid (TFA). For compounds **8**, **16**, and **17**, start from 80% A. For compounds **9–12**, start from 70% A. For compounds **2–6** and **35–44**, start from 60% A. For compounds **13–15**, **21–28**, **45**, and **49–51**, start from 40% A. ¹H NMR and ¹³C NMR spectra were recorded using TMS as an internal standard with Bruker BioSpin Ultrashield 400 NMR system or Varian INOVA 500NB. High resolution mass spectra were recorded on a Shimadzu LCMS-IT-TOF instrument. Cell images were captured on LSM710 confocal microscope from Carl Zeiss and ArrayScanVTI high content screening (HCS) reader from Thermo Fisher. Fluorescence was detected on TECAN Infinite M200 Pro multimode reader and FlexStation 3 multimode reader from Molecular Devices. Apoptosis assay was

conducted by flow cytometer (Beckman Coulter, USA). DMEM high glucose medium, fetal bovine serum, and Hoechst 33342 were purchased from Invitrogen (Life Technologies Corporation, China). HepG2 (ATCCHB-8065), SW480 (ATCCCL-228), and CNE2 (TCHU13) were purchased from National Center for Medical Culture Collection (CMCC). A549/CDDP (BG034), A2780/TAX (BG028), HCT8/VCT (BG208), and MCF7/DOX (BG337) along with their parental cells A549 (BG033), A2780 (BG072), HCT8 (BG207), and MCF7 (BG336) were purchased from Bogoo Biotechnology Co., Ltd. (Shanghai, China). Annexin V/PI apoptosis kit (catalog no. AP101) was purchased from Liankebio Corporation (Guangzhou, China). Tubulin polymerization assay kit (Cytoskeleton, catalog no. BK011P) and Cellomics cytoskeletal rearrangement kit were purchased from Univ-Bio Corporation (Shanghai, China).

2. General Procedure for the Synthesis of 1 and 7. A mixture of 1-(2-bromophenyl)ethanone (1 equiv), corresponding boronic acid (1.3 equiv), dichloro(1,10-bis(diphenylphosphino)ferrocene)-palladium(II)-dichloromethane adduct (0.06 equiv), 2 M K₂CO₃ (1.5 mL), and 1,4-dioxane (1.5 mL) was heated in a sealed vial in a microwave reactor at 150 °C for 20 min. After that, 10 mL of water was added and the mixture was extracted with EtOAc (10 mL) three times. The combined organic layer was washed to neutral and dried over anhydrous sodium sulfate. After removal of the solvent in vacuum, the crude product was purified by column chromatography.

1-(3',4'-Dimethoxy[1,1'-biphenyl]-2-yl)ethanone (1). Yellow liquid, yield 88.02%; ¹H NMR (500 MHz, CDCl₃) δ 7.52–7.47 (m, 2H), 7.41–7.37 (m, 2H), 6.93 (d, *J* = 8.1 Hz, 1H), 6.89 (dd, *J* = 8.1, 2.0 Hz, 1H), 6.87 (d, *J* = 2.0 Hz, 1H), 3.93 (s, 3H), 3.89 (s, 3H), 2.02 (s, 3H); ¹³C NMR (100 MHz, CDCl₃) δ 205.00, 148.86, 148.80, 140.83, 139.94, 133.09, 130.40, 129.80, 127.48, 126.97, 121.14, 111.84, 111.16, 55.72, 55.70, 30.17. HRMS calcd for C₁₆H₁₆O₃ [M + Na]⁺, 279.0997; found, 279.0990.

1-(4'-Fluoro[1,1'-biphenyl]-2-yl)ethanone (7). Yellow liquid, yield 82.15%; ¹H NMR (500 MHz, CDCl₃) δ 7.55 (dd, *J* = 7.6, 1.1 Hz, 1H), 7.51 (td, *J* = 7.5, 1.4 Hz, 1H), 7.42 (td, *J* = 7.5, 1.3 Hz, 1H), 7.36 (dd, *J* = 7.6, 0.9 Hz, 1H), 7.33–7.28 (m, 2H), 7.15–7.09 (m, 2H), 2.05 (s, 3H); ¹³C NMR (100 MHz, CDCl₃) δ 204.40, 163.91, 161.45, 140.79, 139.43, 136.84, 136.80, 130.84, 130.52, 130.44, 130.35, 127.98, 127.63, 115.79, 115.57, 30.41. HRMS calcd for C₁₄H₁₁OF [M + Na]⁺, 237.0692; found, 237.0685.

3. General Procedure for the Synthesis of 2–6 and 8–17. A mixture of the corresponding acetophenone (1 equiv) and aldehyde (1 equiv) in anhydrous EtOH was stirred at room temperature for 10 min. Then solid KOH (6 equiv) was added. The reaction mixture was stirred at room temperature until aldehyde disappeared as monitored by TLC. After that, HCl (10%) was added until pH 4 was obtained. The mixture was concentrated in vacuum to remove EtOH and further extracted with EtOAc. The EtOAc layer was dried over anhydrous sodium sulfate. After removal of the solvent in vacuum, the residue was purified by column chromatography to give corresponding chalcones.

(E)-1-(3',4'-Dimethoxy[1,1'-biphenyl]-2-yl)-3-(4-fluorophenyl)prop-2-en-1-one (2). Yellow oil, yield 30.38%; HPLC *t*_R = 12.23 min; ¹H NMR (400 MHz, CDCl₃) δ 7.63 (ddd, *J* = 7.6, 1.4, 0.5 Hz, 1H), 7.59–7.54 (m, 1H), 7.51–7.48 (m, 1H), 7.48–7.43 (m, 1H), 7.32 (d, *J* = 15.9 Hz, 1H), 7.26–7.21 (m, 2H), 7.01–6.96 (m, 2H), 6.95 (dd, *J* = 8.2, 2.1 Hz, 1H), 6.90 (d, *J* = 2.0 Hz, 1H), 6.88 (d, *J* = 8.2 Hz, 1H), 6.48 (dd, *J* = 15.9, 0.5 Hz, 1H), 3.85 (s, 3H), 3.85 (s, 3H); ¹³C NMR (100 MHz, CDCl₃) δ 196.46, 165.18, 162.68, 149.04, 148.98, 141.94, 140.73, 139.81, 133.26, 131.04, 131.01, 130.81, 130.09, 130.00, 128.83, 127.29, 126.59, 126.57, 121.73, 116.10, 115.89, 112.74, 111.42, 56.05, 56.00. HRMS calcd for C₂₃H₁₉O₃F [M + Na]⁺, 385.1216; found, 385.1209.

(E)-1-(3',4'-Dimethoxy[1,1'-biphenyl]-2-yl)-3-(4-methoxyphenyl)prop-2-en-1-one (3). Yellow oil, yield 31.55%; HPLC *t*_R = 11.44 min; ¹H NMR (400 MHz, CDCl₃) δ 7.59 (dd, *J* = 7.6, 1.0 Hz, 1H), 7.56–7.51 (m, 1H), 7.47 (dd, *J* = 7.7, 0.9 Hz, 1H), 7.45–7.40 (m, 1H), 7.31 (d, *J* = 15.9 Hz, 1H), 7.25–7.19 (m, 2H), 6.94 (dd, *J* = 8.2, 2.1 Hz, 1H), 6.90 (d, *J* = 2.0 Hz, 1H), 6.85 (d, *J* = 8.2 Hz, 1H), 6.83–6.78 (m, 2H), 6.48 (d, *J* = 15.9 Hz, 1H), 3.84 (s, 3H), 3.83 (s, 3H), 3.80 (s, 3H); ¹³C NMR (100 MHz, CDCl₃) δ 196.70, 161.48, 148.83, 148.74,

143.52, 140.47, 139.99, 133.24, 130.38, 129.87, 129.85, 128.57, 127.29, 127.06, 124.69, 121.55, 114.23, 112.60, 111.29, 55.90, 55.85, 55.27. HRMS calcd for $C_{24}H_{22}O_4$ [M + Na]⁺, 397.1416; found, 397.1412.

(*E*)-1-(3',4'-Dimethoxy[1,1'-biphenyl]-2-yl)-3-(3,4-dimethoxyphenyl)prop-2-en-1-one (4). Yellow oil, yield 31.19%; HPLC t_R = 9.25 min; ¹H NMR (400 MHz, CDCl₃) δ 7.63 (dd, *J* = 7.6, 1.1 Hz, 1H), 7.57–7.51 (m, 1H), 7.47 (dd, *J* = 7.7, 1.0 Hz, 1H), 7.46–7.42 (m, 1H), 7.32 (d, *J* = 15.9 Hz, 1H), 6.96–6.92 (m, 2H), 6.89 (dd, *J* = 8.3, 1.9 Hz, 1H), 6.87–6.84 (m, 1H), 6.77 (d, *J* = 8.3 Hz, 1H), 6.71 (d, *J* = 2.0 Hz, 1H), 6.44 (d, *J* = 15.9 Hz, 1H), 3.88 (s, 3H), 3.84 (s, 3H), 3.84 (s, 3H), 3.81 (s, 3H); ¹³C NMR (100 MHz, CDCl₃) δ 196.25, 151.27, 149.13, 148.92, 148.82, 143.36, 140.65, 139.96, 133.37, 130.58, 129.98, 128.80, 127.73, 127.18, 124.93, 123.16, 121.78, 112.55, 111.27, 110.96, 109.27, 55.94, 55.93, 55.90, 55.69. HRMS calcd for $C_{25}H_{24}O_5$ [M + Na]⁺, 427.1521; found, 427.1516.

(*E*)-1-(3',4'-Dimethoxy[1,1'-biphenyl]-2-yl)-3-(2,5-dimethoxyphenyl)prop-2-en-1-one (5). Yellow powder, yield 16.09%; HPLC t_R = 12.15 min; ¹H NMR (400 MHz, CDCl₃) δ 7.71 (d, *J* = 16.1 Hz, 1H), 7.63 (dd, *J* = 7.6, 1.2 Hz, 1H), 7.56–7.51 (m, 1H), 7.49–7.45 (m, 1H), 7.43 (td, *J* = 7.4, 1.3 Hz, 1H), 6.95 (dd, *J* = 8.2, 2.0 Hz, 1H), 6.91 (d, *J* = 1.9 Hz, 1H), 6.87 (d, *J* = 8.2 Hz, 1H), 6.84 (dd, *J* = 9.0, 3.0 Hz, 1H), 6.76 (d, *J* = 9.0 Hz, 1H), 6.64 (d, *J* = 3.0 Hz, 1H), 6.59 (d, *J* = 16.1 Hz, 1H), 3.85 (s, 3H), 3.83 (s, 3H), 3.74 (s, 3H), 3.70 (s, 3H); ¹³C NMR (100 MHz, CDCl₃) δ 196.79, 153.47, 153.05, 148.97, 148.89, 140.73, 140.17, 138.36, 133.42, 130.63, 129.98, 128.91, 127.39, 127.22, 124.37, 121.86, 117.60, 112.78, 112.62, 112.43, 111.35, 56.02, 55.98, 55.94, 55.66. HRMS calcd for $C_{25}H_{24}O_5$ [M + H]⁺, 405.1702; found, 405.1711.

(*E*)-3-(4-Bromophenyl)-1-(3',4'-dimethoxy[1,1'-biphenyl]-2-yl)prop-2-en-1-one (6). Yellow oil, yield 29.08%; HPLC t_R = 16.54 min; ¹H NMR (400 MHz, CDCl₃) δ 7.62 (ddd, *J* = 7.6, 1.4, 0.4 Hz, 1H), 7.58–7.53 (m, 1H), 7.48 (ddd, *J* = 7.8, 1.3, 0.5 Hz, 1H), 7.46–7.42 (m, 1H), 7.42–7.38 (m, 2H), 7.25 (d, *J* = 15.9 Hz, 1H) 7.11–7.06 (m, 2H), 6.93 (dd, *J* = 8.2, 2.1 Hz, 1H), 6.88 (d, *J* = 2.0 Hz, 1H), 6.86 (d, *J* = 8.2 Hz, 1H), 6.51 (d, *J* = 15.9 Hz, 1H), 3.84 (s, 3H), 3.83 (s, 3H); ¹³C NMR (100 MHz, CDCl₃) δ 196.24, 149.04, 149.00, 141.57, 140.75, 139.68, 133.71, 133.17, 132.04, 130.90, 129.98, 129.47, 128.86, 127.30, 127.25, 124.53, 121.75, 112.71, 111.41, 56.04, 55.99. HRMS calcd for $C_{23}H_{19}O_3Br$ [M + Na]⁺, 445.0415; found, 445.0408.

(*E*)-1-(4'-Fluoro[1,1'-biphenyl]-2-yl)-3-(4-methoxyphenyl)prop-2-en-1-one (8). Yellow powder, yield 58.60%; HPLC t_R = 6.91 min; ¹H NMR (500 MHz, CDCl₃) δ 7.61 (dd, *J* = 7.6, 1.4 Hz, 1H), 7.54 (td, *J* = 7.5, 1.4 Hz, 1H), 7.46 (td, *J* = 7.5, 1.2 Hz, 1H), 7.43 (dd, *J* = 7.6, 1.2 Hz, 1H), 7.36–7.32 (m, 2H), 7.31 (d, *J* = 15.9 Hz, 1H), 7.26–7.23 (m, 2H), 7.07–7.02 (m, 2H), 6.85–6.81 (m, 2H), 6.49 (d, *J* = 15.9 Hz, 1H), 3.81 (s, 3H); ¹³C NMR (100 MHz, CDCl₃) δ 196.30, 163.69, 161.68, 161.23, 144.35, 140.00, 139.68, 136.64, 136.61, 130.74, 130.66, 130.50, 130.15, 129.96, 128.68, 127.45, 127.17, 124.62, 115.53, 115.32, 114.34, 55.28. HRMS calcd for $C_{22}H_{17}O_3F$ [M + H]⁺, 333.1291; found, 333.1280.

(*E*)-3-(3,4-Dimethoxyphenyl)-1-(4'-fluoro[1,1'-biphenyl]-2-yl)prop-2-en-1-one (9). Yellow oil, yield 73.90%; HPLC t_R = 6.82 min; ¹H NMR (500 MHz, CDCl₃) δ 7.64 (dd, *J* = 7.6, 1.4 Hz, 1H), 7.55 (td, *J* = 7.5, 1.4 Hz, 1H), 7.46 (td, *J* = 7.5, 1.2 Hz, 1H), 7.43 (dd, *J* = 7.6, 1.2 Hz, 1H), 7.38–7.34 (m, 2H), 7.32 (d, *J* = 15.9 Hz, 1H), 7.08–7.03 (m, 2H), 6.91 (dd, *J* = 8.3, 2.0 Hz, 1H), 6.79 (d, *J* = 8.3 Hz, 1H), 6.74 (d, *J* = 2.0 Hz, 1H), 6.45 (d, *J* = 15.9 Hz, 1H), 3.89 (s, 3H), 3.83 (s, 3H); ¹³C NMR (100 MHz, CDCl₃) δ 196.07, 163.82, 161.36, 151.53, 149.27, 144.39, 140.00, 139.84, 136.80, 136.77, 130.90, 130.82, 130.70, 130.27, 128.91, 127.63, 127.60, 124.92, 123.28, 115.63, 115.42, 111.10, 109.54, 56.03, 55.86. HRMS calcd for $C_{23}H_{19}O_3F$ [M + H]⁺, 363.1396; found, 363.1395.

(*E*)-3-(2,5-Dimethoxyphenyl)-1-(4'-fluoro[1,1'-biphenyl]-2-yl)prop-2-en-1-one (10). Yellow oil, yield 71.55%; HPLC t_R = 8.88 min; ¹H NMR (500 MHz, CDCl₃) δ 7.69 (d, *J* = 16.1 Hz, 1H), 7.63 (dd, *J* = 7.6, 1.1 Hz, 1H), 7.55 (td, *J* = 7.5, 1.4 Hz, 1H), 7.46 (td, *J* = 7.5, 1.3 Hz, 1H), 7.43 (dd, *J* = 7.6, 0.8 Hz, 1H), 7.37–7.33 (m, 2H), 7.07–7.03 (m, 2H), 6.87 (dd, *J* = 9.0, 3.0 Hz, 1H), 6.77 (d, *J* = 9.0 Hz, 1H), 6.68 (d, *J* = 3.0 Hz, 1H), 6.61 (d, *J* = 16.1 Hz, 1H), 3.75 (s, 3H), 3.72 (s, 3H); ¹³C NMR (100 MHz, CDCl₃) δ 196.61, 163.79, 161.33,

153.48, 153.11, 140.07, 139.80, 139.45, 136.75, 136.72, 130.94, 130.86, 130.67, 130.19, 128.92, 127.55, 127.29, 124.09, 117.86, 115.57, 115.35, 112.71, 112.46, 55.97, 55.71. HRMS calcd for $C_{23}H_{19}O_3F$ [M + H]⁺, 363.1396; found, 363.1393.

(*E*)-3-(2,3-Dimethoxyphenyl)-1-(4'-fluoro[1,1'-biphenyl]-2-yl)prop-2-en-1-one (11). Yellow powder, yield 75.00%; HPLC t_R = 8.61 min; ¹H NMR (500 MHz, CDCl₃) δ 7.66 (d, *J* = 16.2 Hz, 1H), 7.61 (dd, *J* = 7.6, 0.8 Hz, 1H), 7.55 (td, *J* = 7.5, 1.3 Hz, 1H), 7.46 (td, *J* = 7.6, 1.1 Hz, 1H), 7.43 (d, *J* = 7.6 Hz, 1H), 7.36–7.33 (m, 2H), 7.08–7.02 (m, 2H), 6.96 (t, *J* = 8.0 Hz, 1H), 6.89 (d, *J* = 8.1 Hz, 1H), 6.79 (d, *J* = 7.9 Hz, 1H), 6.62 (d, *J* = 16.2 Hz, 1H), 3.84 (s, 3H), 3.72 (s, 3H); ¹³C NMR (100 MHz, CDCl₃) δ 196.86, 163.85, 161.39, 153.13, 148.78, 140.05, 139.76, 139.20, 136.67, 136.64, 130.93, 130.85, 130.72, 130.20, 128.84, 128.78, 128.05, 127.59, 124.18, 119.30, 115.69, 115.47, 114.33, 61.29, 55.93. HRMS calcd for $C_{23}H_{19}O_3F$ [M + H]⁺, 363.1396; found, 363.1391.

(*E*)-1-(4'-Fluoro[1,1'-biphenyl]-2-yl)-3-(4-hydroxy-3-methoxyphenyl)prop-2-en-1-one (12). Yellow powder, yield 79.02%; HPLC t_R = 5.23 min; ¹H NMR (500 MHz, CDCl₃) δ 7.63 (dd, *J* = 7.6, 1.4 Hz, 1H), 7.55 (td, *J* = 7.5, 1.4 Hz, 1H), 7.46 (td, *J* = 7.5, 1.3 Hz, 1H), 7.43 (dd, *J* = 7.6, 1.2 Hz, 1H), 7.36–7.33 (m, 2H), 7.30 (d, *J* = 15.9 Hz, 1H), 7.07–7.03 (m, 2H), 6.87 (dd, *J* = 8.2, 1.7 Hz, 1H), 6.84 (d, *J* = 8.2 Hz, 1H), 6.74 (d, *J* = 1.7 Hz, 1H), 6.44 (d, *J* = 15.9 Hz, 1H), 5.86 (s, 1H), 3.86 (s, 3H); ¹³C NMR (100 MHz, CDCl₃) δ 196.29, 163.83, 161.37, 148.50, 146.91, 144.83, 139.99, 139.85, 136.82, 136.79, 130.92, 130.84, 130.70, 130.28, 128.91, 127.61, 127.20, 124.66, 123.79, 115.64, 115.43, 114.86, 109.30, 55.94. HRMS calcd for $C_{22}H_{17}O_3F$ [M + H]⁺, 349.1240; found, 349.1229.

(*E*)-1-(4'-Fluoro[1,1'-biphenyl]-2-yl)-3-(3-hydroxy-4-methoxyphenyl)prop-2-en-1-one (13). Yellow crystals, yield 67.38%; HPLC t_R = 16.79 min; ¹H NMR (400 MHz, CDCl₃) δ 7.60 (dd, *J* = 7.6, 1.3 Hz, 1H), 7.54 (td, *J* = 7.5, 1.4 Hz, 1H), 7.46 (dd, *J* = 7.5, 1.2 Hz, 1H), 7.42 (d, *J* = 7.5 Hz, 1H), 7.36–7.30 (m, 2H), 7.26 (d, *J* = 15.9 Hz, 1H), 7.08–7.01 (m, 2H), 6.88 (d, *J* = 2.0 Hz, 1H), 6.84 (dd, *J* = 8.3, 2.0 Hz, 1H), 6.77 (d, *J* = 8.3 Hz, 1H), 6.46 (d, *J* = 15.9 Hz, 1H), 5.64 (s, 1H), 3.89 (s, 3H); ¹³C NMR (100 MHz, CDCl₃) δ 196.58, 163.68, 161.22, 149.08, 145.92, 144.78, 139.91, 139.69, 136.58, 136.54, 130.72, 130.64, 130.54, 130.15, 128.65, 127.99, 127.44, 125.00, 122.15, 115.54, 115.33, 113.29, 110.64, 55.90. HRMS calcd for $C_{22}H_{17}O_3F$ [M + H]⁺, 349.1234; found, 349.1219.

(*E*)-5-(3-(4'-Fluoro[1,1'-biphenyl]-2-yl)-3-oxoprop-1-en-1-yl)-2-methoxyphenylboronic Acid (14). Light yellow powder, yield 70.45%; HPLC t_R = 15.67 min; ¹H NMR (400 MHz, CDCl₃) δ 7.79 (d, *J* = 2.3 Hz, 1H), 7.60 (d, *J* = 7.6 Hz, 1H), 7.57–7.52 (m, 1H), 7.48–7.39 (m, 3H), 7.36–7.28 (m, 3H), 7.03 (t, *J* = 8.7 Hz, 2H), 6.86 (d, *J* = 8.7 Hz, 1H), 6.56 (d, *J* = 16.0 Hz, 1H), 5.81 (s, 2H), 3.93 (s, 3H); ¹³C NMR (100 MHz, DMSO) δ 195.47, 165.31, 162.92, 160.49, 144.67, 139.64, 139.02, 136.63, 135.64, 132.04, 130.75, 130.67, 130.47, 130.17, 128.20, 127.50, 126.18, 124.31, 115.39, 115.18, 110.84, 55.56. HRMS calcd for $C_{22}H_{18}O_4BF$ [M + H]⁺, 377.1359; found, 377.1354.

(*E*)-3-(4-(Dimethylamino)phenyl)-1-(4'-fluoro[1,1'-biphenyl]-2-yl)prop-2-en-1-one (15). Yellow powder, yield 67.26%; HPLC t_R = 20.87 min; ¹H NMR (400 MHz, DMSO) δ 7.61–7.56 (m, 1H), 7.54–7.49 (m, 2H), 7.46 (d, *J* = 7.6 Hz, 1H), 7.39–7.30 (m, 4H), 7.23–7.14 (m, 3H), 6.64 (d, *J* = 8.8 Hz, 2H), 6.53 (d, *J* = 15.9 Hz, 1H), 2.96 (s, 6H); ¹³C NMR (100 MHz, CDCl₃) δ 196.73, 163.58, 161.13, 152.05, 146.18, 140.38, 139.49, 136.75, 136.71, 130.65, 130.57, 130.20, 130.10, 128.52, 127.31, 122.02, 121.91, 115.39, 115.18, 111.70, 39.93. HRMS calcd for $C_{23}H_{20}NOF$ [M + H]⁺, 346.1602; found, 346.1590.

(*E*)-1-(4'-Fluoro[1,1'-biphenyl]-2-yl)-3-(5-methylfuran-2-yl)prop-2-en-1-one (16). Yellow oil, yield 40.84%; HPLC t_R = 7.11 min; ¹H NMR (500 MHz, CDCl₃) δ 7.58 (dd, *J* = 7.6, 1.0 Hz, 1H), 7.52 (td, *J* = 7.5, 1.4 Hz, 1H), 7.43 (td, *J* = 7.6, 1.3 Hz, 1H), 7.41 (dd, *J* = 7.7, 0.7 Hz, 1H), 7.33–7.30 (m, 2H), 7.03 (d, *J* = 15.7 Hz, 1H), 7.06–7.01 (m, 2H), 6.45 (d, *J* = 3.3 Hz, 1H), 6.45 (d, *J* = 15.7 Hz, 1H), 6.04 (dd, *J* = 3.3, 0.8 Hz, 1H), 2.29 (s, 3H); ¹³C NMR (100 MHz, CDCl₃) δ 196.18, 163.82, 161.37, 156.22, 149.81, 140.06, 139.80, 136.68, 136.65, 130.87, 130.81, 130.73, 130.47, 130.30, 128.60, 127.48, 122.75, 117.98, 115.59, 115.37, 109.38, 13.96. HRMS calcd for $C_{20}H_{15}O_2F$ [M + H]⁺, 307.1134; found, 307.1123.

(*E*)-1-(4'-Fluoro[1,1'-biphenyl]-2-yl)-3-(thiophen-2-yl)prop-2-en-1-one (**17**). Yellow oil, yield 19.48%; HPLC t_R = 6.98 min; ^1H NMR (500 MHz, CDCl_3) δ 7.63 (dd, J = 7.6, 1.2 Hz, 1H), 7.55 (td, J = 7.5, 1.4 Hz, 1H), 7.49 (d, J = 15.6 Hz, 1H), 7.47 (td, J = 7.5, 1.3 Hz, 1H), 7.43 (dd, J = 7.6, 1.0 Hz, 1H), 7.35–7.31 (m, 3H), 7.13 (d, J = 3.6 Hz, 1H), 7.08–7.04 (m, 2H), 6.99 (dd, J = 5.1, 3.6 Hz, 1H), 6.37 (d, J = 15.6 Hz, 1H); ^{13}C NMR (100 MHz, CDCl_3) δ 195.41, 163.84, 161.38, 140.00, 139.91, 139.72, 136.52, 136.48, 136.24, 131.64, 130.83, 130.80, 130.74, 130.25, 129.06, 128.82, 128.27, 127.57, 125.58, 115.67, 115.45. HRMS calcd for $\text{C}_{19}\text{H}_{13}\text{OFS}$ $[\text{M} + \text{H}]^+$, 309.0749; found, 309.0739.

4. General Procedure for the Synthesis of 18–20 and 29–34. These intermediate chalcones were synthesized by the Claisen–Schmidt condensation. In general, acetophenone (5 equiv) was added to equimolar of aromatic aldehyde and dissolved in EtOH. To the solution, 6 M NaOH (aq) (2 mL) was added, and the reaction mixture was stirred at room temperature until the aldehyde disappeared, by monitoring with TLC. Then HCl (10%) was added until pH 4 was obtained. The mixture was concentrated in vacuum to remove EtOH and further extracted with EtOAc. The EtOAc layer was dried over anhydrous sodium sulfate. After removal of the solvent in vacuum, the crude product was purified by recrystallization with EtOH to give corresponding chalcones.

(*E*)-1-(2-Bromophenyl)-3-(4-methoxyphenyl)prop-2-en-1-one (**18**). Light yellow crystal, yield 85.68%; HPLC t_R = 11.76 min; ^1H NMR (400 MHz, CDCl_3) δ 7.64 (d, J = 7.9 Hz, 1H), 7.51 (d, J = 8.8 Hz, 2H), 7.43–7.29 (m, 3H), 7.38 (d, J = 16.0 Hz, 1H), 6.97 (d, J = 16.0 Hz, 1H), 6.92 (d, J = 8.8 Hz, 2H), 3.85 (s, 3H).

(*E*)-1-(2-Bromophenyl)-3-(3,4-dimethoxyphenyl)prop-2-en-1-one (**19**). Light green crystal, yield 86.94%; HPLC t_R = 9.12 min; ^1H NMR (400 MHz, CDCl_3) δ 7.68–7.62 (m, 1H), 7.43–7.30 (m, 3H), 7.35 (d, J = 16.0 Hz, 1H), 7.13 (dd, J = 8.3, 2.0 Hz, 1H), 7.08 (d, J = 1.9 Hz, 1H), 6.96 (d, J = 16.0 Hz, 1H), 6.87 (d, J = 8.3 Hz, 1H), 3.92 (s, 3H), 3.91 (s, 3H). HRMS calcd for $\text{C}_{17}\text{H}_{15}\text{O}_3\text{Br}$ $[\text{M} + \text{H}]^+$, 347.0277; found, 347.0283.

(*E*)-1-(2-Bromophenyl)-3-(3-hydroxy-4-methoxyphenyl)prop-2-en-1-one (**20**). Light yellow crystal, yield 65.70%; HPLC t_R = 13.30 min; ^1H NMR (400 MHz, CDCl_3) δ 7.63 (d, J = 7.8 Hz, 1H), 7.43–7.28 (m, 4H), 7.17 (d, J = 1.8 Hz, 1H), 7.05 (dd, J = 8.3, 1.6 Hz, 1H), 6.94 (d, J = 16.0 Hz, 1H), 6.85 (d, J = 8.3 Hz, 1H), 5.72 (s, 1H), 3.93 (s, 3H); ^{13}C NMR (100 MHz, CDCl_3) δ 194.90, 149.43, 147.11, 146.05, 141.25, 133.37, 131.24, 129.09, 127.84, 127.32, 124.28, 122.79, 119.42, 113.54, 110.76, 56.04. HRMS calcd for $\text{C}_{16}\text{H}_{13}\text{O}_3\text{Br}$ $[\text{M} + \text{H}]^+$, 333.0121; found, 333.0115.

(*E*)-3-(2-Bromophenyl)-1-(4-methoxyphenyl)prop-2-en-1-one (**29**). White solid, yield 41.04%; HPLC t_R = 14.23 min; ^1H NMR (400 MHz, CDCl_3) δ 8.11 (d, J = 15.7 Hz, 1H), 8.04 (d, J = 8.8 Hz, 2H), 7.73 (d, J = 7.8 Hz, 1H), 7.64 (d, J = 8.0 Hz, 1H), 7.43 (d, J = 15.7 Hz, 1H), 7.36 (t, J = 7.4 Hz, 1H), 7.24 (t, J = 7.5 Hz, 1H), 6.99 (d, J = 8.8 Hz, 2H), 3.90 (s, 3H).

(*E*)-3-(2-Bromophenyl)-1-(3,4-dimethoxyphenyl)prop-2-en-1-one (**30**). Yellow crystal, yield 77.93%; HPLC t_R = 11.73 min; ^1H NMR (400 MHz, CDCl_3) δ 8.11 (d, J = 15.7 Hz, 1H), 7.73 (dd, J = 7.7, 1.1 Hz, 1H), 7.68 (dd, J = 8.4, 2.0 Hz, 1H), 7.64 (dd, J = 8.0, 0.9 Hz, 1H), 7.62 (d, J = 1.9 Hz, 1H), 7.43 (d, J = 15.7 Hz, 1H), 7.36 (t, J = 7.3 Hz, 1H), 7.27–7.21 (m, 1H), 6.94 (d, J = 8.4 Hz, 1H), 3.97 (s, 6H). HRMS calcd for $\text{C}_{17}\text{H}_{15}\text{O}_3\text{Br}$ $[\text{M} + \text{H}]^+$, 347.0277; found, 347.0267.

(*E*)-3-(2-Bromophenyl)-1-(3-hydroxyphenyl)prop-2-en-1-one (**31**). Yellow solid, yield 62.65%; HPLC t_R = 8.73 min; ^1H NMR (400 MHz, CDCl_3) δ 8.14 (d, J = 15.7 Hz, 1H), 7.72 (d, J = 7.8 Hz, 1H), 7.64 (d, J = 7.8 Hz, 1H), 7.58–7.56 (m, 2H), 7.40 (d, J = 15.6 Hz, 1H), 7.44–7.33 (m, 2H), 7.27–7.23 (m, 1H), 7.15–7.08 (m, 1H).

(*E*)-3-(2-Bromophenyl)-1-(4-hydroxy-3-methoxyphenyl)prop-2-en-1-one (**32**). Yellow powder, yield 76.59%; HPLC t_R = 8.67 min; ^1H NMR (400 MHz, CDCl_3) δ 8.10 (d, J = 15.7 Hz, 1H), 7.73 (dd, J = 7.8, 1.6 Hz, 1H), 7.66–7.61 (m, 3H), 7.43 (d, J = 15.6 Hz, 1H), 7.38–7.33 (m, 1H), 7.24 (td, J = 7.5, 1.6 Hz, 1H), 7.01–6.97 (m, 1H), 6.15 (s, 1H), 3.99 (s, 3H). HRMS calcd for $\text{C}_{16}\text{H}_{13}\text{O}_3\text{Br}$ $[\text{M} + \text{H}]^+$, 333.0121; found, 333.0112.

(*E*)-3-(2-Bromophenyl)-1-(3-hydroxy-4-methoxyphenyl)prop-2-en-1-one (**33**). Yellow solid, yield 78.94%; HPLC t_R = 8.53 min; ^1H NMR (400 MHz, CDCl_3) δ 8.11 (d, J = 15.6 Hz, 1H), 7.72 (dd, J =

7.8, 1.6 Hz, 1H), 7.67–7.61 (m, 3H), 7.42 (d, J = 15.6 Hz, 1H), 7.36 (t, J = 7.6 Hz, 1H), 7.24 (td, J = 7.5, 1.9 Hz, 1H), 6.97–6.92 (m, 1H), 5.70 (s, 1H), 3.99 (s, 3H); ^{13}C NMR (100 MHz, CDCl_3) δ 188.79, 150.93, 145.77, 142.49, 135.33, 133.60, 131.63, 131.24, 127.97, 127.78, 125.88, 124.91, 122.38, 114.91, 110.16, 56.22. HRMS calcd for $\text{C}_{16}\text{H}_{13}\text{O}_3\text{Br}$ $[\text{M} + \text{H}]^+$, 333.0121; found, 333.0118.

(*E*)-3-(2-Bromophenyl)-1-(3,4,5-trimethoxyphenyl)prop-2-en-1-one (**34**). Light yellow crystal, yield 85.28%; HPLC t_R = 21.35 min; ^1H NMR (400 MHz, acetone) δ 8.12 (d, J = 15.5 Hz, 1H), 8.03 (d, J = 7.8 Hz, 1H), 7.84 (d, J = 15.5 Hz, 1H), 7.73 (d, J = 8.0 Hz, 1H), 7.46 (d, J = 9.6 Hz, 3H), 7.42–7.35 (m, 1H), 3.94 (s, 6H), 3.84 (s, 3H).

5. General Procedure for the Synthesis of 21–28 and 35–45. These compounds were synthesized using Suzuki–Miyaura coupling conditions as previously described in the synthesis of **1** and **7**, in which a mixture of corresponding intermediate chalcones (1.0 mmol), corresponding boronic acid (1.3 mmol), dichloro(1,10-bis(diphenylphosphino)ferrocene)palladium(II)–dichloromethane adduct (0.06 mmol), 2 M K_2CO_3 (1.5 mL), and 1,4-dioxane (1.5 mL) was used.

(*E*)-1-(3'-Fluoro[1,1'-biphenyl]-2-yl)-3-(4-methoxyphenyl)prop-2-en-1-one (**21**). Orange oil, yield 69.04%; HPLC t_R = 22.38 min; ^1H NMR (400 MHz, CDCl_3) δ 7.62 (dd, J = 7.5, 1.4 Hz, 1H), 7.56 (td, J = 7.5, 1.5 Hz, 1H), 7.48 (dd, J = 7.5, 1.3 Hz, 1H), 7.44 (d, J = 7.5 Hz, 1H), 7.34–7.28 (m, 1H), 7.31 (d, J = 15.9 Hz, 1H), 7.24–7.27 (m, 2H), 7.15–7.08 (m, 2H), 6.98 (ddd, J = 10.1, 7.7, 2.2 Hz, 1H), 6.86–6.80 (m, 2H), 6.52 (d, J = 15.9 Hz, 1H), 3.81 (s, 3H); ^{13}C NMR (100 MHz, CDCl_3) δ 196.00, 163.86, 161.67, 161.41, 144.47, 142.83, 142.76, 139.94, 139.46, 139.44, 130.51, 130.02, 130.00, 129.95, 129.92, 128.69, 127.77, 127.12, 125.00, 124.97, 124.54, 115.99, 115.78, 114.52, 114.31, 55.22. HRMS calcd for $\text{C}_{22}\text{H}_{17}\text{O}_2\text{F}$ $[\text{M} + \text{H}]^+$, 333.1285; found, 333.1281.

(*E*)-1-(2-(6-Fluoropyridin-3-yl)phenyl)-3-(4-methoxyphenyl)prop-2-en-1-one (**22**). Yellow powder, yield 80.65%; HPLC t_R = 18.09 min; ^1H NMR (400 MHz, CDCl_3) δ 8.23 (d, J = 2.5 Hz, 1H), 7.76 (ddd, J = 8.4, 7.7, 2.6 Hz, 1H), 7.64 (dd, J = 7.5, 1.2 Hz, 1H), 7.58 (td, J = 7.5, 1.5 Hz, 1H), 7.52 (td, J = 7.5, 1.3 Hz, 1H), 7.42 (dd, J = 7.6, 0.9 Hz, 1H), 7.37–7.31 (m, 2H), 7.34 (d, J = 16.0 Hz, 1H), 6.90 (dd, J = 8.4, 3.0 Hz, 1H), 6.88–6.83 (m, 2H), 6.64 (d, J = 16.0 Hz, 1H), 3.83 (s, 3H); ^{13}C NMR (100 MHz, CDCl_3) δ 195.09, 163.90, 161.71, 161.52, 146.86, 146.71, 145.48, 141.45, 141.37, 139.71, 135.63, 134.13, 134.09, 130.45, 130.22, 129.91, 128.49, 127.93, 126.60, 124.03, 114.21, 108.90, 108.53, 55.04. HRMS calcd for $\text{C}_{21}\text{H}_{16}\text{NO}_2\text{F}$ $[\text{M} + \text{H}]^+$, 334.1238; found, 334.1244.

(*E*)-3-(4-Methoxyphenyl)-1-(2-(pyridin-3-yl)phenyl)prop-2-en-1-one (**23**). Yellow oil, yield 68.23%; HPLC t_R = 6.53 min; ^1H NMR (400 MHz, CDCl_3) δ 8.65 (d, J = 0.9 Hz, 1H), 8.53 (d, J = 4.8 Hz, 1H), 7.69–7.63 (m, 2H), 7.59 (t, J = 7.5 Hz, 1H), 7.51 (t, J = 7.5 Hz, 1H), 7.45 (d, J = 7.6 Hz, 1H), 7.33 (d, J = 15.9 Hz, 1H), 7.30–7.25 (m, 3H), 6.83 (d, J = 8.6 Hz, 2H), 6.56 (d, J = 15.9 Hz, 1H), 3.79 (d, J = 9.2 Hz, 3H); ^{13}C NMR (100 MHz, CDCl_3) δ 195.10, 161.46, 149.00, 148.28, 144.86, 139.71, 136.74, 135.97, 135.93, 130.35, 130.04, 129.73, 128.46, 127.73, 126.58, 124.06, 122.76, 114.03, 54.93. HRMS calcd for $\text{C}_{21}\text{H}_{17}\text{NO}_2$ $[\text{M} + \text{H}]^+$, 316.1332; found, 316.1320.

(*E*)-3-(3,4-Dimethoxyphenyl)-1-(3'-fluoro[1,1'-biphenyl]-2-yl)prop-2-en-1-one (**24**). Orange oil, yield 72.36%; HPLC t_R = 19.82 min; ^1H NMR (400 MHz, CDCl_3) δ 7.65 (dd, J = 7.6, 1.3 Hz, 1H), 7.56 (td, J = 7.5, 1.4 Hz, 1H), 7.49 (dd, J = 7.5, 1.2 Hz, 1H), 7.47–7.43 (m, 1H), 7.34–7.27 (m, 1H), 7.31 (d, J = 15.9 Hz, 1H), 7.16–7.11 (m, 2H), 6.99 (ddd, J = 8.1, 2.9, 1.5 Hz, 1H), 6.91 (dd, J = 8.3, 1.9 Hz, 1H), 6.79 (d, J = 8.3 Hz, 1H), 6.75 (d, J = 1.9 Hz, 1H), 6.48 (d, J = 15.9 Hz, 1H), 3.88 (s, 3H), 3.83 (s, 3H); ^{13}C NMR (100 MHz, CDCl_3) δ 194.82, 163.43, 160.97, 151.09, 148.79, 143.80, 142.61, 142.53, 139.52, 139.08, 139.06, 130.18, 129.64, 129.61, 129.53, 128.39, 127.41, 127.05, 124.78, 124.75, 124.27, 122.81, 115.57, 115.35, 114.06, 113.86, 110.70, 109.14, 55.32, 55.22. HRMS calcd for $\text{C}_{23}\text{H}_{19}\text{O}_3\text{F}$ $[\text{M} + \text{H}]^+$, 363.1391; found, 363.1393.

(*E*)-3-(3,4-Dimethoxyphenyl)-1-(2-(6-fluoropyridin-3-yl)phenyl)prop-2-en-1-one (**25**). Orange oil, yield 68.62%; HPLC t_R = 15.29 min; ^1H NMR (400 MHz, CDCl_3) δ 8.23 (s, 1H), 7.80–7.73 (m, 1H), 7.65 (d, J = 7.5 Hz, 1H), 7.59 (t, J = 7.3 Hz, 1H), 7.52 (t, J = 7.4 Hz,

1H), 7.42 (d, $J = 7.5$ Hz, 1H), 7.33 (d, $J = 15.9$ Hz, 1H), 6.98 (d, $J = 8.2$ Hz, 1H), 6.90 (dd, $J = 8.4, 2.7$ Hz, 1H), 6.86 (s, 1H), 6.82 (d, $J = 8.3$ Hz, 1H), 6.62 (d, $J = 15.9$ Hz, 1H), 3.90 (s, 3H), 3.86 (s, 3H); ^{13}C NMR (100 MHz, CDCl_3) δ 194.82, 163.69, 161.31, 151.39, 148.85, 146.60, 146.45, 145.58, 141.40, 141.32, 139.40, 135.45, 134.02, 133.98, 130.35, 130.05, 128.36, 127.77, 126.73, 124.01, 122.99, 110.78, 109.44, 108.75, 108.38, 55.39, 55.32. HRMS calcd for $\text{C}_{22}\text{H}_{18}\text{NO}_3\text{F}$ $[\text{M} + \text{H}]^+$, 364.1343; found, 364.1350.

(*E*)-1-(3'-Fluoro[1,1'-biphenyl]-2-yl)-3-(3-hydroxy-4-methoxyphenyl)prop-2-en-1-one (**26**). Yellow oil, yield 72.38%; HPLC $t_{\text{R}} = 16.75$ min; ^1H NMR (400 MHz, CDCl_3) δ 7.61 (d, $J = 7.5$ Hz, 1H), 7.54 (dd, $J = 7.5, 1.2$ Hz, 1H), 7.48 (dd, $J = 7.4, 1.0$ Hz, 1H), 7.44 (d, $J = 7.7$ Hz, 1H), 7.33–7.29 (m, 1H), 7.26 (d, $J = 15.9$ Hz, 1H), 7.15–7.11 (m, 1H), 7.09 (d, $J = 9.7$ Hz, 1H), 6.98 (td, $J = 8.5, 1.5$ Hz, 1H), 6.88 (s, 1H), 6.84 (d, $J = 8.3$ Hz, 1H), 6.77 (d, $J = 8.3$ Hz, 1H), 6.50 (d, $J = 15.9$ Hz, 1H), 5.65 (s, 1H), 3.89 (s, 3H); ^{13}C NMR (100 MHz, CDCl_3) δ 196.66, 163.65, 161.20, 149.32, 145.84, 145.39, 142.57, 142.49, 139.49, 139.31, 139.30, 130.50, 129.91, 129.84, 128.51, 127.62, 127.56, 124.77, 124.74, 124.56, 122.16, 115.80, 115.59, 114.37, 114.17, 113.35, 110.61, 55.59. HRMS calcd for $\text{C}_{22}\text{H}_{17}\text{O}_3\text{F}$ $[\text{M} + \text{H}]^+$, 349.1234; found, 349.1230.

(*E*)-3-(3-Hydroxy-4-methoxyphenyl)-1-(3',4',5'-trimethoxy[1,1'-biphenyl]-2-yl)prop-2-en-1-one (**27**). Yellow oil, yield 79.14%; HPLC $t_{\text{R}} = 14.01$ min; ^1H NMR (400 MHz, CDCl_3) δ 7.61 (d, $J = 7.6$ Hz, 1H), 7.56–7.51 (m, 1H), 7.50–7.41 (m, 2H), 7.26 (d, $J = 15.4$ Hz, 1H), 6.84–6.77 (m, 2H), 6.74 (d, $J = 8.3$ Hz, 1H), 6.59 (s, 2H), 6.45 (d, $J = 15.4$ Hz, 1H), 5.66 (s, 1H), 3.87 (s, 3H), 3.80 (s, 6H), 3.77 (d, $J = 0.5$ Hz, 3H); ^{13}C NMR (100 MHz, CDCl_3) δ 196.41, 152.74, 149.08, 145.75, 143.76, 140.34, 139.49, 137.36, 135.78, 130.15, 129.29, 128.15, 127.44, 127.05, 124.40, 121.57, 113.05, 110.43, 106.48, 60.27, 55.74, 55.35. HRMS calcd for $\text{C}_{23}\text{H}_{24}\text{O}_6$ $[\text{M} + \text{H}]^+$, 421.1646; found, 421.1653.

(*E*)-3-(3-Hydroxy-4-methoxyphenyl)-1-(2',3',4'-trimethoxy[1,1'-biphenyl]-2-yl)prop-2-en-1-one (**28**). Yellow powder, yield 62.75%; HPLC $t_{\text{R}} = 15.13$ min; ^1H NMR (400 MHz, DMSO) δ 9.11 (s, 1H), 7.63–7.55 (m, 2H), 7.47 (td, $J = 7.5, 1.1$ Hz, 1H), 7.38 (d, $J = 7.6$ Hz, 1H), 7.23 (d, $J = 15.8$ Hz, 1H), 6.94–6.81 (m, 5H), 6.51 (d, $J = 15.8$ Hz, 1H), 3.78 (s, 3H), 3.77 (s, 3H), 3.55 (s, 3H), 3.50 (s, 3H); ^{13}C NMR (100 MHz, CDCl_3) δ 194.80, 153.68, 151.10, 148.76, 145.82, 142.94, 142.02, 140.04, 136.99, 130.80, 130.46, 128.44, 128.27, 127.43, 127.08, 124.95, 124.09, 122.08, 112.81, 110.43, 107.37, 60.56, 60.50, 55.88, 55.73. HRMS calcd for $\text{C}_{25}\text{H}_{24}\text{O}_6$ $[\text{M} + \text{H}]^+$, 421.1646; found, 421.1655.

(*E*)-3-(4'-Fluoro[1,1'-biphenyl]-2-yl)-1-(4-methoxyphenyl)prop-2-en-1-one (**35**). Light yellow powder, yield 80.23%; HPLC $t_{\text{R}} = 17.89$ min; ^1H NMR (400 MHz, CDCl_3) δ 7.98 (d, $J = 8.8$ Hz, 2H), 7.82 (d, $J = 7.1$ Hz, 1H), 7.78 (d, $J = 15.8$ Hz, 1H), 7.49–7.39 (m, 3H), 7.36 (d, $J = 7.4$ Hz, 1H), 7.31 (dd, $J = 8.4, 5.5$ Hz, 2H), 7.13 (t, $J = 8.6$ Hz, 2H), 6.96 (d, $J = 8.8$ Hz, 2H), 3.88 (s, 3H); ^{13}C NMR (100 MHz, CDCl_3) δ 188.65, 163.73, 163.53, 161.28, 142.89, 142.30, 136.09, 133.44, 131.52, 131.44, 130.89, 130.64, 129.99, 127.86, 127.14, 123.40, 115.48, 115.26, 113.90, 55.50. HRMS calcd for $\text{C}_{22}\text{H}_{17}\text{O}_2\text{F}$ $[\text{M} + \text{H}]^+$, 333.1285; found, 333.1282.

(*E*)-3-(2-(6-Fluoropyridin-3-yl)phenyl)-1-(4-methoxyphenyl)prop-2-en-1-one (**36**). White powder, yield 75.68%; HPLC $t_{\text{R}} = 11.99$ min; ^1H NMR (400 MHz, CDCl_3) δ 8.22 (d, $J = 2.4$ Hz, 1H), 8.03–7.94 (m, 2H), 7.89–7.82 (m, 1H), 7.80–7.73 (m, 1H), 7.69 (d, $J = 15.5$ Hz, 1H), 7.53–7.44 (m, 2H), 7.48 (d, $J = 15.6$ Hz, 1H), 7.40–7.33 (m, 1H), 7.02 (dd, $J = 8.4, 2.8$ Hz, 1H), 7.00–6.92 (m, 2H), 3.89 (s, 3H); ^{13}C NMR (100 MHz, CDCl_3) δ 188.25, 164.39, 163.65, 162.00, 148.01, 147.86, 142.43, 142.35, 141.60, 138.19, 133.89, 133.82, 133.78, 130.91, 130.81, 130.70, 130.24, 128.80, 127.39, 124.31, 113.98, 109.42, 109.04, 55.57. HRMS calcd for $\text{C}_{21}\text{H}_{16}\text{NO}_2\text{F}$ $[\text{M} + \text{H}]^+$, 334.1238; found, 334.1238.

(*E*)-1-(3,4-Dimethoxyphenyl)-3-(4'-fluoro[1,1'-biphenyl]-2-yl)prop-2-en-1-one (**37**). Light yellow powder, yield 83.56%; HPLC $t_{\text{R}} = 15.29$ min; ^1H NMR (400 MHz, CDCl_3) δ 7.82 (d, $J = 8.1$ Hz, 1H), 7.79 (d, $J = 15.2$ Hz, 1H), 7.62 (dd, $J = 8.5, 1.7$ Hz, 1H), 7.57 (d, $J = 1.6$ Hz, 1H), 7.49–7.41 (m, 3H), 7.37 (dd, $J = 6.8, 1.7$ Hz, 1H), 7.34–7.29 (m, 2H), 7.13 (t, $J = 8.6$ Hz, 2H), 6.90 (d, $J = 8.5$ Hz, 1H), 3.97

(s, 3H), 3.94 (s, 3H); ^{13}C NMR (100 MHz, CDCl_3) δ 188.11, 163.56, 161.10, 153.24, 149.17, 142.65, 142.12, 135.99, 135.96, 133.25, 131.38, 131.30, 131.04, 130.48, 129.84, 127.71, 127.07, 122.98, 122.92, 115.31, 115.10, 110.70, 109.93, 55.93, 55.85. HRMS calcd for $\text{C}_{22}\text{H}_{19}\text{O}_3\text{F}$ $[\text{M} + \text{H}]^+$, 363.1391; found, 363.1382.

(*E*)-1-(3,4-Dimethoxyphenyl)-3-(2-(6-fluoropyridin-3-yl)phenyl)prop-2-en-1-one (**38**). White powder, yield 76.38%; HPLC $t_{\text{R}} = 11.98$ min; ^1H NMR (400 MHz, CDCl_3) δ 8.22 (s, 1H), 7.91–7.82 (m, 1H), 7.76 (td, $J = 8.0, 2.4$ Hz, 1H), 7.70 (d, $J = 15.5$ Hz, 1H), 7.62 (d, $J = 8.4$ Hz, 1H), 7.56 (d, $J = 1.4$ Hz, 1H), 7.52–7.42 (m, 3H), 7.40–7.32 (m, 1H), 7.02 (dd, $J = 8.3, 2.8$ Hz, 1H), 6.91 (d, $J = 8.4$ Hz, 1H), 3.96 (s, 3H), 3.95 (s, 3H); ^{13}C NMR (100 MHz, CDCl_3) δ 188.00, 164.31, 161.92, 153.47, 149.33, 147.94, 147.80, 142.35, 142.27, 141.55, 138.10, 133.78, 133.75, 133.71, 130.96, 130.63, 130.18, 128.72, 127.37, 123.97, 123.13, 110.78, 110.05, 109.33, 108.96, 56.09, 56.00. HRMS calcd for $\text{C}_{22}\text{H}_{18}\text{NO}_3\text{F}$ $[\text{M} + \text{H}]^+$, 364.1343; found, 364.1334.

(*E*)-3-(4'-Fluoro[1,1'-biphenyl]-2-yl)-1-(3-hydroxyphenyl)prop-2-en-1-one (**39**). White powder, yield 74.69%; HPLC $t_{\text{R}} = 11.55$ min; ^1H NMR (400 MHz, acetone) δ 8.67 (s, 1H), 8.09 (dd, $J = 7.5, 1.6$ Hz, 1H), 7.75 (d, $J = 15.6$ Hz, 1H), 7.70 (d, $J = 15.6$ Hz, 1H), 7.61–7.57 (m, 1H), 7.56–7.49 (m, 3H), 7.46–7.40 (m, 3H), 7.37 (t, $J = 7.9$ Hz, 1H), 7.31–7.24 (m, 2H), 7.10 (ddd, $J = 8.1, 2.6, 0.9$ Hz, 1H); ^{13}C NMR (100 MHz, acetone) δ 189.91, 164.50, 162.06, 158.62, 143.16, 143.13, 140.50, 137.28, 137.25, 133.92, 132.62, 132.54, 131.36, 131.02, 130.60, 128.86, 128.04, 124.29, 120.82, 120.74, 116.12, 115.91, 115.64. HRMS calcd for $\text{C}_{21}\text{H}_{15}\text{O}_2\text{F}$ $[\text{M} + \text{H}]^+$, 319.1129; found, 319.1131.

(*E*)-3-(2-(6-Fluoropyridin-3-yl)phenyl)-1-(3-hydroxyphenyl)prop-2-en-1-one (**40**). White powder, yield 71.42%; HPLC $t_{\text{R}} = 7.13$ min; ^1H NMR (400 MHz, acetone) δ 8.67 (s, 1H), 8.24 (s, 1H), 8.16–8.11 (m, 1H), 8.00 (td, $J = 8.1, 2.5$ Hz, 1H), 7.76 (d, $J = 15.6$ Hz, 1H), 7.68 (d, $J = 15.6$ Hz, 1H), 7.63–7.52 (m, 3H), 7.52–7.46 (m, 2H), 7.37 (t, $J = 7.9$ Hz, 1H), 7.24 (dd, $J = 8.4, 2.9$ Hz, 1H), 7.11 (dd, $J = 8.1, 1.8$ Hz, 1H); ^{13}C NMR (100 MHz, acetone) δ 189.71, 165.24, 162.89, 158.67, 148.90, 148.75, 143.78, 143.70, 142.26, 140.41, 139.30, 134.95, 134.90, 134.43, 131.58, 131.23, 130.65, 129.66, 128.30, 125.06, 120.94, 120.79, 115.66, 110.11, 109.73. HRMS calcd for $\text{C}_{20}\text{H}_{14}\text{NO}_2\text{F}$ $[\text{M} + \text{H}]^+$, 320.1081; found, 320.1078.

(*E*)-3-(4'-Fluoro[1,1'-biphenyl]-2-yl)-1-(4-hydroxy-3-methoxyphenyl)prop-2-en-1-one (**41**). Yellow powder, yield 76.98%; HPLC $t_{\text{R}} = 11.31$ min; ^1H NMR (400 MHz, CDCl_3) δ 7.82 (d, $J = 7.1$ Hz, 1H), δ 7.79 (d, $J = 15.6$ Hz, 1H), 7.62–7.56 (m, 2H), 7.45 (d, $J = 15.5$ Hz, 1H), 7.48–7.41 (m, 2H), 7.36 (dd, $J = 7.1, 1.7$ Hz, 1H), 7.34–7.28 (m, 2H), 7.13 (t, $J = 8.6$ Hz, 2H), 6.97 (d, $J = 8.0$ Hz, 1H), 6.09 (s, 1H), 3.96 (s, 3H); ^{13}C NMR (100 MHz, CDCl_3) δ 188.55, 163.77, 161.32, 150.65, 147.05, 142.98, 142.35, 136.16, 136.12, 133.48, 131.55, 131.47, 130.89, 130.70, 130.04, 127.89, 127.25, 123.86, 123.18, 115.52, 115.30, 113.96, 110.66, 56.15. HRMS calcd for $\text{C}_{22}\text{H}_{17}\text{O}_3\text{F}$ $[\text{M} + \text{H}]^+$, 349.1234; found, 349.1233.

(*E*)-3-(2-(6-Fluoropyridin-3-yl)phenyl)-1-(4-hydroxy-3-methoxyphenyl)prop-2-en-1-one (**42**). Yellow powder, yield 70.38%; HPLC $t_{\text{R}} = 7.12$ min; ^1H NMR (400 MHz, CDCl_3) δ 8.22 (d, $J = 2.4$ Hz, 1H), 7.85 (dd, $J = 6.2, 3.0$ Hz, 1H), 7.80–7.74 (m, 1H), 7.71 (d, $J = 15.5$ Hz, 1H), 7.60 (dd, $J = 8.2, 1.9$ Hz, 1H), 7.58 (d, $J = 1.8$ Hz, 1H), 7.53–7.47 (m, 3H), 7.38–7.34 (m, 1H), 7.02 (dd, $J = 8.4, 2.6$ Hz, 1H), 6.98 (d, $J = 8.1$ Hz, 1H), 6.18 (s, 1H), 3.96 (s, 3H); ^{13}C NMR (100 MHz, DMSO) δ 186.88, 163.70, 161.34, 152.09, 147.80, 147.69, 147.54, 143.13, 143.05, 139.90, 137.80, 133.75, 133.70, 133.06, 130.60, 130.19, 129.28, 128.66, 127.55, 123.87, 123.78, 115.05, 111.74, 109.42, 109.05, 55.69. HRMS calcd for $\text{C}_{21}\text{H}_{16}\text{NO}_3\text{F}$ $[\text{M} + \text{H}]^+$, 350.1187; found, 350.1181.

(*E*)-3-(4'-Fluoro[1,1'-biphenyl]-2-yl)-1-(3-hydroxy-4-methoxyphenyl)prop-2-en-1-one (**43**). Yellow crystals, yield 77.54%; HPLC $t_{\text{R}} = 11.35$ min; ^1H NMR (400 MHz, CDCl_3) δ 7.81 (dd, $J = 7.4, 1.8$ Hz, 1H), 7.76 (d, $J = 15.7$ Hz, 1H), 7.57 (d, $J = 1.4$ Hz, 1H), 7.56 (dd, $J = 7.6, 1.8$ Hz, 1H), 7.48–7.39 (m, 2H), 7.42 (d, $J = 15.5$ Hz, 1H), 7.38–7.34 (m, 1H), 7.33–7.27 (m, 2H), 7.17–7.10 (m, 2H), 6.93–6.88 (m, 1H), 5.70 (s, 1H), 3.97 (s, 3H); ^{13}C NMR (100 MHz, CDCl_3) δ 188.92, 163.77, 161.32, 150.76, 145.70, 142.98, 142.37, 136.14, 136.11, 133.47, 131.78, 131.55, 131.47, 130.67, 130.02, 127.89,

127.15, 123.48, 122.14, 115.53, 115.31, 114.85, 110.12, 56.16. HRMS calcd for $C_{22}H_{17}O_3F$ $[M + H]^+$, 349.1234; found, 349.1231.

(*E*)-3-(2-(6-Fluoropyridin-3-yl)phenyl)-1-(3-hydroxy-4-methoxyphenyl)prop-2-en-1-one (**44**). Yellow powder, yield 70.05%; HPLC t_R = 7.12 min; 1H NMR (400 MHz, $CDCl_3$) δ 8.22 (d, J = 2.6 Hz, 1H), 7.88–7.82 (m, 1H), 7.76 (td, J = 7.9, 2.6 Hz, 1H), 7.67 (d, J = 15.6 Hz, 1H), 7.59–7.55 (m, 2H), 7.53–7.48 (m, 2H), 7.44 (d, J = 15.5 Hz, 1H), 7.38–7.34 (m, 1H), 7.03 (dd, J = 8.3, 2.9 Hz, 1H), 6.92 (d, J = 9.1 Hz, 1H), 5.71 (s, 1H), 3.98 (s, 3H); ^{13}C NMR (100 MHz, DMSO) δ 187.24, 163.68, 161.32, 152.38, 147.68, 147.53, 146.64, 143.20, 143.12, 139.96, 137.87, 133.73, 133.68, 132.95, 130.65, 130.48, 130.27, 128.71, 127.47, 123.75, 121.87, 114.78, 111.16, 109.45, 109.08, 55.74. HRMS calcd for $C_{21}H_{16}NO_3F$ $[M + H]^+$, 350.1187; found, 350.1185.

(*E*)-3-(4'-Fluoro[1,1'-biphenyl]-2-yl)-1-(3,4,5-trimethoxyphenyl)prop-2-en-1-one (**45**). Light yellow crystals, yield 81.42%; HPLC t_R = 24.13 min; 1H NMR (400 MHz, $CDCl_3$) δ 7.82 (d, J = 15.7 Hz, 1H), 7.81 (d, J = 7.2 Hz, 1H), 7.50–7.41 (m, 2H), 7.41–7.35 (m, 2H), 7.32 (d, J = 8.7 Hz, 1H), 7.30 (d, J = 8.4 Hz, 1H), 7.22 (s, 2H), 7.13 (t, J = 8.7 Hz, 2H), 3.93 (s, 3H), 3.92 (s, 6H); ^{13}C NMR (100 MHz, $CDCl_3$) δ 188.58, 163.64, 161.18, 153.11, 143.45, 142.60, 142.24, 136.05, 136.02, 133.26, 133.13, 131.41, 131.33, 130.66, 130.07, 127.80, 127.41, 122.99, 115.42, 115.20, 106.11, 60.88, 56.31. HRMS calcd for $C_{24}H_{21}O_4F$ $[M + Na]^+$, 415.1316; found, 415.1308.

6. General Procedure for the Synthesis of 49–51. 2-Bromobenzoic acid (5 mmol) was refluxed in 10 mL of $SOCl_2$ for 1 h and then concentrated in vacuum to remove the solvent $SOCl_2$. The remainder in 20 mL of anhydrous toluene was added dropwise to a mixture of phenylamine (5 mmol) and triethylamine (5 mmol) in 20 mL of toluene, and then the mixture was refluxed for 12 h. After cooling, the mixture was evaporated to remove toluene and extracted by $CHCl_3$ from 10% HCl and 5% $NaHCO_3$ three times. The combined organic layer was dried over anhydrous sodium sulfate. After removal of $CHCl_3$ in vacuum, the crude product was purified by column chromatography to yield the intermediates **46–48**.

2-Bromo-*N*-(4-methoxybenzyl)benzamide (**46**). White solid, yield 71.21%; HPLC t_R = 10.83 min; 1H NMR (400 MHz, acetone) δ 7.82 (s, 1H), 7.61 (d, J = 7.9 Hz, 1H), 7.46–7.30 (m, 5H), 6.89 (d, J = 8.4 Hz, 2H), 4.52 (d, J = 6.0 Hz, 2H), 3.78 (s, 3H); ^{13}C NMR (100 MHz, $CDCl_3$) δ 167.48, 158.96, 137.79, 133.20, 131.04, 129.85, 129.32, 129.23, 127.37, 119.30, 113.99, 55.22, 43.45. HRMS calcd for $C_{15}H_{14}NO_2Br$ $[M + Na]^+$, 342.0100; found, 342.0092.

2-Bromo-*N*-(3,4-dimethoxybenzyl)benzamide (**47**). White solid, yield 73.54%; HPLC t_R = 8.58 min; 1H NMR (400 MHz, $CDCl_3$) δ 7.58 (d, J = 8.0 Hz, 1H), 7.55 (dd, J = 7.6, 0.9 Hz, 1H), 7.35 (t, J = 7.4 Hz, 1H), 7.28–7.24 (m, 1H), 6.95 (s, 1H), 6.91 (d, J = 8.2 Hz, 1H), 6.83 (d, J = 8.1 Hz, 1H), 6.23 (s, 1H), 4.59 (d, J = 5.6 Hz, 2H), 3.88 (s, 3H), 3.87 (s, 3H); ^{13}C NMR (100 MHz, $CDCl_3$) δ 167.55, 149.32, 148.69, 137.84, 133.44, 131.34, 130.41, 129.61, 127.63, 120.37, 119.36, 111.50, 111.37, 56.03, 44.06. HRMS calcd for $C_{16}H_{16}NO_3Br$ $[M + Na]^+$, 372.0206; found, 372.0202.

2-Bromo-*N*-(3,4,5-trimethoxybenzyl)benzamide (**48**). White solid, yield 68.82%; HPLC t_R = 8.85 min; 1H NMR (400 MHz, $CDCl_3$) δ 7.59 (d, J = 8.0 Hz, 1H), 7.55 (d, J = 7.6 Hz, 1H), 7.36 (t, J = 7.4 Hz, 1H), 7.30–7.26 (m, 1H), 6.61 (s, 2H), 6.30 (s, 1H), 4.58 (d, J = 5.7 Hz, 2H), 3.85 (s, 6H), 3.82 (s, 3H); ^{13}C NMR (100 MHz, $CDCl_3$) δ 167.60, 153.54, 137.88, 137.65, 133.53, 133.49, 131.39, 129.63, 127.67, 119.39, 105.23, 60.88, 56.30, 44.45. HRMS calcd for $C_{17}H_{18}NO_4Br$ $[M + Na]^+$, 402.0311; found, 402.0296.

49–51 was synthesized using Suzuki–Miyaura coupling conditions as previously described in the synthesis of **1** and **7**, in which a mixture of **46–48** (1.0 mmol), (4-fluorophenyl)boronic acid (1.3 mmol), dichloro(1,10-bis(diphenylphosphino)ferrocene)palladium(II)–dichloromethane adduct (0.06 mmol), 2 M K_2CO_3 (1.5 mL), and 1,4-dioxane (1.5 mL) was used.

4'-Fluoro-*N*-(4-methoxybenzyl)[1,1'-biphenyl]-2-carboxamide (**49**). White powder, yield 80.26%; HPLC t_R = 14.56 min; 1H NMR (400 MHz, acetone) δ 7.52–7.35 (m, 7H), 7.11–7.00 (m, 4H), 6.84–6.76 (m, 2H), 4.30 (d, J = 6.0 Hz, 2H), 3.78 (s, 3H); ^{13}C NMR (100 MHz, $CDCl_3$) δ 169.18, 163.69, 161.24, 158.96, 138.43, 136.17,

136.13, 135.98, 130.34, 130.26, 130.10, 129.97, 129.69, 129.12, 128.50, 127.59, 115.53, 115.31, 113.89, 55.21, 43.40. HRMS calcd for $C_{21}H_{18}NO_2F$ $[M + H]^+$, 336.1394; found, 336.1399.

N-(3,4-Dimethoxybenzyl)-4'-fluoro[1,1'-biphenyl]-2-carboxamide (**50**). White powder, yield 83.48%; HPLC t_R = 12.15 min; 1H NMR (400 MHz, $CDCl_3$) δ 7.68 (d, J = 7.3 Hz, 1H), 7.50–7.44 (m, 1H), 7.41 (t, J = 7.4 Hz, 1H), 7.37–7.29 (m, 3H), 7.01 (t, J = 8.6 Hz, 2H), 6.73 (d, J = 8.2 Hz, 1H), 6.62 (s, 1H), 6.49 (d, J = 8.1 Hz, 1H), 5.43 (s, 1H), 4.28 (d, J = 5.5 Hz, 2H), 3.86 (s, 3H), 3.82 (s, 3H); ^{13}C NMR (100 MHz, $CDCl_3$) δ 169.12, 163.50, 161.04, 148.85, 148.36, 138.28, 135.99, 135.96, 135.78, 130.22, 130.14, 130.01, 129.91, 128.37, 127.46, 120.12, 115.34, 115.12, 111.38, 111.11, 55.76, 55.70, 43.74. HRMS calcd for $C_{22}H_{20}NO_3F$ $[M + Na]^+$, 388.1319; found, 388.1302.

4'-Fluoro-*N*-(3,4,5-trimethoxybenzyl)[1,1'-biphenyl]-2-carboxamide (**51**). White powder, yield 85.61%; HPLC t_R = 12.42 min; 1H NMR (400 MHz, $CDCl_3$) δ 7.68 (d, J = 7.7 Hz, 1H), 7.49–7.37 (m, 2H), 7.37–7.28 (m, 3H), 7.01 (t, J = 8.5 Hz, 2H), 6.29 (s, 2H), 5.51 (s, 1H), 4.25 (d, J = 5.6 Hz, 2H), 3.81 (s, 3H), 3.79 (s, 6H); ^{13}C NMR (100 MHz, $CDCl_3$) δ 169.26, 163.48, 161.03, 153.14, 138.31, 137.28, 135.99, 135.96, 135.68, 133.24, 130.27, 130.19, 130.09, 130.03, 128.38, 127.51, 115.31, 115.10, 105.16, 60.60, 55.93, 44.36. HRMS calcd for $C_{23}H_{22}NO_4F$ $[M + Na]^+$, 418.1425; found, 418.1417.

7. Biology. Cell Culture. Cells (A549, CNE2, SW480, MCF-7, HepG2, A2780, A2780/TAX, HCT-8, HCT-8/VCT, A549/CDDP, and MCF-7/DOX) were grown in tissue culture flasks in complete growth medium (DMEM high glucose medium, pH 7.4, supplemented with 10% fetal bovine serum, 100 mg/mL streptomycin, and 100 units/mL penicillin) in a carbon dioxide incubator (37 °C, 5% CO_2 , 90% relative humidity (RH)).

8. SRB Cell Survival Assay. Cytotoxicity study was determined using a 96-well microplate. SRB assay was performed to evaluate cell viability.²⁴ It measured cellular protein content to determine cell density. Cells were plated at 5000 cells/well. The cells were allowed to grow in carbon dioxide incubator (37 °C, 5% CO_2 , 90% RH) for 24 h. Then one plate (plate day 0) was directly fixed by trichloroacetic acid (50%, 50 μ L) by means described in the following text. Meanwhile different concentrations of test compounds in complete growth medium (100 μ L) were added to other plates in triplicate, and these plates were further incubated for 48 h. The cell growth was stopped by gently layering trichloroacetic acid (50%, 50 μ L) on top of the medium in all the wells. The plates were incubated at 4 °C for 1 h to fix the cells attached to the bottom of the wells. The liquid of all the wells was gently pipetted out and discarded. The plates were washed five times with distilled water and air-dried. The plates were stained with SRB dye (0.4% in 1% acetic acid, 100 μ L) for 30 min. The plates were washed five times with 1% acetic acid and then air-dried. The adsorbed dye was dissolved in Tris base solution (150 μ L, 10 mM, pH 10.4), and plates were gently shaken for 1 h on an orbital shaker. The optical density (OD) was recorded on a TECAN Infinite M200 Pro multimode reader at 515 nm. The cell growth was determined by subtracting mean OD value of plate day 0 from the mean OD value of experimental set. From a plot of % control of cell viability against the test compound concentration by plot concentrations on a log scale and a fit of the data by using nonlinear regression in GraphPad Prism 5, the compound concentration required to inhibit tumor cell proliferation by 50% (IC_{50}) was obtained from the dose–response curves. All data are average values from triplicate samples, and the experiments were repeated at least two times.

9. Cell Cycle Analysis. A549 cells were plated at 5000/well in a 96-well microplate and cultured overnight. Then various concentrations of tested compounds were added for 24 h. Cells were then fixed with prewarmed (37 °C) paraformaldehyde for 10 min. Then cells were permeabilized with permeabilization buffer (Triton X-100) for 10 min and washed twice with PBS. Hoechst 33342 was added and incubated at room temperature for 1 h. After washing, 50 μ L of PBS was added and the plates were evaluate on an ArrayScan HCS reader.²⁵

10. Apoptosis Assay. Annexin V/PI apoptosis kit was used. A549 cells (5×10^4 /well) was incubated in six-well plate for 24 h. Different concentrations of **15** (0.25, 0.50, 0.75, 1.0 μ M) and 0.25 μ M

colchicine as control were added to cultured A549 cells and incubated for 48 h. Approximately 1×10^5 cells were then stained for 5 min at room temperature in the dark with fluorescein isothiocyanate (FITC) conjugated annexin V (5 μ L) and propidium iodide (PI) (10 μ L) in a 1X annexin-binding buffer and analyzed by a two-color flow cytometric assay. Annexin V and PI emissions were detected in the FL1 and FL2 channels of flow cytometer, respectively. Flow cytometer data show three distinct populations of cells. The normal healthy cells, early apoptosis, late apoptosis, and necrotic populations were represented by annexin V-negative/PI-negative population, annexin V-positive/PI-negative, annexin V-positive/PI-positive, and annexin V-negative/PI-positive cells, respectively. The data were analyzed using Cell Quest program from Beckman Coulter.²⁶

11. In Vitro Tubulin Polymerization Assay. Tubulin polymerization assay kit was used, and the enclosed experimental protocol was followed. Tubulin (20 μ M, 99% pure, 50 μ L) was mixed with different concentrations of tested compounds (10X in distilled water, 5 μ L) in general tubulin buffer (80 mM PIPES, pH 6.9, 2.0 mM MgCl₂, and 0.5 mM EGTA), containing 1 mM GTP, 20% glycerol, and fluorescent reporter DAPI.²⁷ Microtubule polymerization was immediately monitored in a kinetic model of FlexStation 3 multimode reader followed by an increase in fluorescence emission at 450 nm at 37 °C (excitation wavelength is 360 nm). Each compound was tested in duplicate at each concentration in each experiment.²⁸

12. Immunofluorescence Microscopy. Cellomics cytoskeletal rearrangement kit was used, and the experiment protocol with slight modification was followed. A549 cells were plated in a confocal culture dish at 6×10^4 cells/dish and grown for 24 h. Tested compound **26** was added for 24 h, and then the dishes were placed in ice for 1 h to make the microtubule depolymerized. After that, dishes were reincubated in 37 °C incubator for 0, 5, 10, and 15 min to observe whether the microtubule could reassemble. Cells were then fixed with prewarmed (37 °C) paraformaldehyde for 15 min. Then cells were permeabilized with permeabilization buffer (Triton X-100) for 15 min and washed twice with PBS. Mouse anti-tubulin antibody was added and incubated at room temperature for 1 h. Cells were washed three times and incubated with DyLight 549-conjugated goat anti-mouse IgG along with DAPI (stain nucleus) kept in darkness at room temperature for 30 min. After washing, 1 mL PBS was added and fluorescently stained cells were analyzed by confocal microscope.¹⁷

13. Fluorescence Measurement. Tubulin was incubated without or with different concentrations of **15** and **26** in tubulin general buffer and immediately evaluated in a FlexStation 3 multimode reader. The fluorescence was found to increase when **15** and **26** were added to tubulin, but no obvious fluorescence increase was observed in the tubulin only control group. The optimal excitation wavelength and the optimal emission wavelength were evaluated by a fluorescence wavelength scanning model in Flexstation 3 multimode reader.²⁹

14. Competitive Inhibition Assay. Tubulin–**15** complex was formed by incubating 4 μ M tubulin in general tubulin buffer with 8 μ M **15** at 37 °C in a kinetic model of FlexStation 3 multimode reader (excitation at 430 nm, emission at 510 nm) until the fluorescence of tubulin–**15** came to a stable level. **26**, colchicine, and vincristine (0–80 μ M) were added to the preformed tubulin–**15** complex, and fluorescence was again determined at 37 °C using FlexStation 3 multimode reader (excitation at 430 nm, emission at 510 nm).^{20,29}

15. Tumor Xenografts Growth Inhibition Assay. All animal experiments complied with the Zhongshan School of Medicine Policy on the Care and Use of Laboratory Animals. Female BALB/c nude mice (5 weeks old) were purchased from the Experimental Animal Center at Sun Yat-Sen University and maintained in pathogen-free conditions. A549 cells were harvested during log-phase growth and resuspended in RPMI-1640 medium at 6.67×10^7 cells/mL. Each mouse was injected subcutaneously in the right flank with 1×10^7 cells. When the tumor volume reached approximately 100 mm³, the mice were randomly divided into two groups of eight animals and treated intraperitoneally (ip) with **26** at a dose of 2 mg/kg body weight every other day for 2 weeks, whereas the control group was treated with an equivalent volume of normal saline (including 0.5% DMSO, 5% Kolliphor HS 15). Tumor size and body weight were

measured everyday. The tumor volume was calculated using the formula $V = (\text{larger diameter}) \times (\text{smaller diameter})^2/2$, and growth curves were plotted using average tumor volume within each experimental group at the set time points. At the end of treatment, the animals were sacrificed, and the tumors were removed and weighed.

■ ASSOCIATED CONTENT

📄 Supporting Information

Rho123 accumulation and efflux assay; affinity-induced fluorescence by **15** and **26**; inhibition of affinity-induced fluorescence by DTNB; ¹H NMR, ¹³C NMR, HRMS, and HPLC spectra of final compounds. This material is available free of charge via the Internet at <http://pubs.acs.org>.

■ AUTHOR INFORMATION

Corresponding Author

*Phone and fax: 020-39943054. E-mail: phsbxzh@mail.sysu.edu.cn.

Author Contributions

[†]C.Z. and Y.Z. contribute equally.

Notes

The authors declare no competing financial interest.

■ ACKNOWLEDGMENTS

We are indebted to the National Nature Science Foundation of China (Grants 30973619 and 81172931) and the Fundamental Research Funds for the Central Universities (Grant 09ykpy66) of China for financial support of this study.

■ ABBREVIATIONS USED

Rho123, rhodamine 123; NF- κ B, nuclear factor κ B; SRB, sulforhodamine B; TAX, Taxol; VCT, vincristine; CDDP, cisplatin; DOX, doxorubicin; DRI, drug resistance index; RH, relative humidity; DTNB, 5,5'-dithiobis(2-nitrobenzoic acid)

■ REFERENCES

- (1) (a) Jordan, M. A.; Wilson, L. Microtubules as a target for anticancer drugs. *Nat. Rev. Cancer* **2004**, *4* (4), 253–265. (b) Downing, K. H.; Nogales, E. Tubulin structure: insights into microtubule properties and functions. *Curr. Opin. Struct. Biol.* **1998**, *8* (6), 785–791. (c) Nogales, E. Structural insights into microtubule function. *Annu. Rev. Biophys. Biomol. Struct.* **2001**, *30* (1), 397–420.
- (2) Risinger, A. L.; Giles, F. J.; Mooberry, S. L. Microtubule dynamics as a target in oncology. *Cancer Treat. Rev.* **2009**, *35* (3), 255–261.
- (3) (a) Xu, W.; Xi, B.; Wu, J.; An, H.; Zhu, J.; Abassi, Y.; Feinstein, S. C.; Gaylord, M.; Geng, B.; Yan, H.; Fan, W.; Sui, M.; Wang, X.; Xu, X. Natural product derivative bis(4-fluorobenzyl)trisulfide inhibits tumor growth by modification of β -tubulin at Cys 12 and suppression of microtubule dynamics. *Mol. Cancer Ther.* **2009**, *8* (12), 3318–3330. (b) Kerssemakers, J. W. J.; Munteanu, E. L.; Laan, L.; Noetzel, T. L.; Janson, M. E.; Dogterom, M. Assembly dynamics of microtubules at molecular resolution. *Nature* **2006**, *442* (7103), 709–712.
- (4) (a) Romagnoli, R.; Baraldi, P. G.; Lopez-Cara, C.; Preti, D.; Aghazadeh Tabrizi, M.; Balzarini, J.; Bassetto, M.; Brancale, A.; Fu, X.-H.; Gao, Y.; Li, J.; Zhang, S.-Z.; Hamel, E.; Bortolozzi, R.; Basso, G.; Viola, G. Concise synthesis and biological evaluation of 2-aroil-5-amino benzo[b]thiophene derivatives as a novel class of potent antimetastatic agents. *J. Med. Chem.* **2013**, *56* (22), 9296–9309. (b) Reddy, M. V. R.; Mallireddigari, M. R.; Pallela, V. R.; Cosenza, S. C.; Billa, V. K.; Akula, B.; Subbaiah, D. R. C. V.; Bharathi, E. V.; Padgaonkar, A.; Lv, H.; Gallo, J. M.; Reddy, E. P. Design, synthesis, and biological evaluation of (E)-N-aryl-2-arylethenesulfonamide analogues as potent and orally bioavailable microtubule-targeted anticancer agents. *J. Med. Chem.* **2013**, *56* (13), 5562–5586.

- (5) Stanton, R. A.; Gernert, K. M.; Nettles, J. H.; Aneja, R. Drugs that target dynamic microtubules: a new molecular perspective. *Med. Res. Rev.* **2011**, *31* (3), 443–481.
- (6) Dumontet, C.; Jordan, M. A. Microtubule-binding agents: a dynamic field of cancer therapeutics. *Nat. Rev. Drug. Discovery* **2010**, *9* (10), 790–803.
- (7) (a) Cutts, J. H.; Beer, C. T.; Noble, R. L. Biological properties of vincalukoblastine, an alkaloid in *Vinca rosea* Linn, with reference to its antitumor action. *Cancer Res.* **1960**, *20* (7,Part 1), 1023–1031. (b) Noble, R. L.; Beer, C. T.; Cutts, J. H. Role of chance observations in chemotherapy: *Vinca rosea*. *Ann. N.Y. Acad. Sci.* **1958**, *76* (3), 882–894.
- (8) (a) Schiff, P. B.; Fant, J.; Horwitz, S. B. Promotion of microtubule assembly in vitro by Taxol. *Nature* **1979**, *277* (5698), 665–667. (b) Wani, M. C.; Taylor, H. L.; Wall, M. E.; Coggon, P.; McPhail, A. T. Plant antitumor agents. VI. Isolation and structure of Taxol, a novel antileukemic and antitumor agent from *Taxus brevifolia*. *J. Am. Chem. Soc.* **1971**, *93* (9), 2325–2327.
- (9) (a) Norris, B.; Pritchard, K. I.; James, K.; Myles, J.; Bennett, K.; Marlin, S.; Skillings, J.; Findlay, B.; Vandenberg, T.; Goss, P.; Latreille, J.; Rudinkas, L.; Lofters, W.; Trudeau, M.; Osoba, D.; Rodgers, A. Phase III comparative study of vinorelbine combined with doxorubicin versus doxorubicin alone in disseminated metastatic/recurrent breast cancer: National Cancer Institute of Canada clinical trials group study MA8. *J. Clin. Oncol.* **2000**, *18* (12), 2385–2394. (b) Pajk, B.; Cufer, T.; Canney, P.; Ellis, P.; Cameron, D.; Blot, E.; Vermorken, J.; Coleman, R.; Marreaud, S.; Bogaerts, J.; Basaran, G.; Piccart, M. Anti-tumor activity of capecitabine and vinorelbine in patients with anthracycline- and taxane-pretreated metastatic breast cancer: findings from the EORTC 10001 randomized phase II trial. *Breast* **2008**, *17* (2), 180–185.
- (10) (a) Rustin, G. J. S.; Galbraith, S. M.; Anderson, H.; Stratford, M.; Folkes, L. K.; Sena, L.; Gumbrell, L.; Price, P. M. Phase I clinical trial of weekly combretastatin A4 phosphate: clinical and pharmacokinetic results. *J. Clin. Oncol.* **2003**, *21* (15), 2815–2822. (b) Nathan, P.; Zweifel, M.; Padhani, A. R.; Koh, D.-M.; Ng, M.; Collins, D. J.; Harris, A.; Carden, C.; Smythe, J.; Fisher, N.; Taylor, N. J.; Stirling, J. J.; Lu, S.-P.; Leach, M. O.; Rustin, G. J. S.; Judson, I. Phase I trial of combretastatin A4 phosphate (CA4P) in combination with bevacizumab in patients with advanced cancer. *Clin. Cancer Res.* **2012**, *18* (12), 3428–3439. (c) Zweifel, M.; Jayson, G. C.; Reed, N. S.; Osborne, R.; Hassan, B.; Ledermann, J.; Shreeves, G.; Poupard, L.; Lu, S.-P.; Balkissoon, J.; Chaplin, D. J.; Rustin, G. J. S. Phase II trial of combretastatin A4 phosphate, carboplatin, and paclitaxel in patients with platinum-resistant ovarian cancer. *Ann. Oncol.* **2011**, *22* (9), 2036–2041.
- (11) (a) Fojo, A. T.; Menefee, M. Microtubule targeting agents: Basic mechanisms of multidrug resistance (MDR). *Semin. Oncol.* **2005**, *32* (Suppl. 7), 3–8. (b) Sahenk, Z.; Barohn, R.; New, P.; Mendell, J. R. Taxol neuropathy: electrodiagnostic and sural nerve biopsy findings. *Arch. Neurol.* **1994**, *51* (7), 726–729.
- (12) Ammon, H. P. T.; Wahl, M. A. Pharmacology of *Curcuma longa*. *Planta Med.* **1991**, *57*, 1–7.
- (13) (a) Itokawa, H.; Shi, Q.; Akiyama, T.; Morris-Natschke, S. L.; Lee, K.-H. Recent advances in the investigation of curcuminoids. *Chin. Med.* **2008**, *3* (11), 1–13. (b) Chakraborti, S.; Das, L.; Kapoor, N.; Das, A.; Dwivedi, V.; Poddar, A.; Chakraborti, G.; Janik, M.; Basu, G.; Panda, D.; Chakraborti, P.; Surolia, A.; Bhattacharyya, B. Curcumin recognizes a unique binding site of tubulin. *J. Med. Chem.* **2011**, *54* (18), 6183–6196.
- (14) (a) Zuo, Y.; Huang, J.; Zhou, B.; Wang, S.; Shao, W.; Zhu, C.; Lin, L.; Wen, G.; Wang, H.; Du, J.; Bu, X. Synthesis, cytotoxicity of new 4-arylidene curcumin analogues and their multi-functions in inhibition of both NF- κ B and Akt signalling. *Eur. J. Med. Chem.* **2012**, *55*, 346–357. (b) Qiu, X.; Du, Y.; Lou, B.; Zuo, Y.; Shao, W.; Huo, Y.; Huang, J.; Yu, Y.; Zhou, B.; Du, J.; Fu, H.; Bu, X. Synthesis and identification of new 4-arylidene curcumin analogues as potential anticancer agents targeting nuclear factor- κ B signaling pathway. *J. Med. Chem.* **2010**, *53* (23), 8260–8273.
- (15) Zuo, Y.; Yu, Y.; Wang, S.; Shao, W.; Zhou, B.; Lin, L.; Luo, Z.; Huang, R.; Du, J.; Bu, X. Synthesis and cytotoxicity evaluation of biaryl-based chalcones and their potential in TNF α -induced nuclear factor- κ B activation inhibition. *Eur. J. Med. Chem.* **2012**, *50*, 393–404.
- (16) (a) Ducki, S.; Rennison, D.; Woo, M.; Kendall, A.; Chabert, J. F. D.; McGown, A. T.; Lawrence, N. J. Combretastatin-like chalcones as inhibitors of microtubule polymerization. Part I: Synthesis and biological evaluation of antivascular activity. *Bioorg. Med. Chem.* **2009**, *17* (22), 7698–7710. (b) Kim, D. Y.; Kim, K.-H.; Kim, N. D.; Lee, K. Y.; Han, C. K.; Yoon, J. H.; Moon, S. K.; Lee, S. S.; Seong, B. L. Design and biological evaluation of novel tubulin inhibitors as antimetabolic agents using a pharmacophore binding model with tubulin. *J. Med. Chem.* **2006**, *49* (19), 5664–5670.
- (17) Voigt, T.; Gerding-Reimers, C.; Ngoc Tran, T. T.; Bergmann, S.; Lachance, H.; Schölermann, B.; Brockmeyer, A.; Janning, P.; Ziegler, S.; Waldmann, H. A natural product inspired tetrahydropyran collection yields mitosis modulators that synergistically target CSE1L and tubulin. *Angew. Chem., Int. Ed.* **2013**, *52* (1), 410–414.
- (18) (a) Yang, H.; Ganguly, A.; Cabral, F. Inhibition of cell migration and cell division correlates with distinct effects of microtubule inhibiting drugs. *J. Biol. Chem.* **2010**, *285* (42), 32242–32250. (b) Rai, A.; Surolia, A.; Panda, D. An antitubulin agent BCFMT inhibits proliferation of cancer cells and induces cell death by inhibiting microtubule dynamics. *PLoS One* **2012**, *7* (8), e44311.
- (19) Bhattacharyya, B.; Wolff, J. Promotion of fluorescence upon binding of colchicine to tubulin. *Proc. Natl. Acad. Sci. U.S.A.* **1974**, *71* (7), 2627–2631.
- (20) Tong, Y.-G.; Zhang, X.-W.; Geng, M.-Y.; Yue, J.-M.; Xin, X.-L.; Tian, F.; Shen, X.; Tong, L.-J.; Li, M.-H.; Zhang, C.; Li, W.-H.; Lin, L.-P.; Ding, J. Pseudolarix acid B, a new tubulin-binding agent, inhibits angiogenesis by interacting with a novel binding site on tubulin. *Mol. Pharmacol.* **2006**, *69* (4), 1226–1233.
- (21) Beyer, C. F.; Zhang, N.; Hernandez, R.; Vitale, D.; Lucas, J.; Nguyen, T.; Discafani, C.; Ayril-Kaloustian, S.; Gibbons, J. J. TTI-237: A novel microtubule-active compound with in vivo antitumor activity. *Cancer Res.* **2008**, *68* (7), 2292–2300.
- (22) (a) Lin, W.; Yuan, L.; Cao, Z.; Feng, Y.; Long, L. A sensitive and selective fluorescent thiol probe in water based on the conjugate 1,4-addition of thiols to α,β -unsaturated ketones. *Chem.—Eur. J.* **2009**, *15* (20), 5096–5103. (b) Khatik, G. L.; Kumar, R.; Chakraborti, A. K. Catalyst-free conjugated addition of thiols to α,β -unsaturated carbonyl compounds in water. *Org. Lett.* **2006**, *8* (11), 2433–2436.
- (23) (a) Gireesh, K. K.; Rashid, A.; Chakraborti, S.; Panda, D.; Manna, T. CIL-102 binds to tubulin at colchicine binding site and triggers apoptosis in MCF-7 cells by inducing monopolar and multinucleated cells. *Biochem. Pharmacol.* **2012**, *84* (5), 633–645. (b) Luduena, R. F.; Roach, M. C. Tubulin sulfhydryl groups as probes and targets for antimetabolic and antimicrotubule agents. *Pharmacol. Ther.* **1991**, *49* (1–2), 133–152.
- (24) (a) Skehan, P.; Storeng, R.; Scudiero, D.; Monks, A.; McMahon, J.; Vistica, D.; Warren, J. T.; Bokesch, H.; Kenney, S.; Boyd, M. R. New colorimetric cytotoxicity assay for anticancer-drug screening. *J. Natl. Cancer Inst.* **1990**, *82* (13), 1107–1112. (b) Vichai, V.; Kirtikara, K. Sulforhodamine B colorimetric assay for cytotoxicity screening. *Nat. Protoc.* **2006**, *1* (3), 1112–1116.
- (25) Jensen, N. A.; Gerth, K.; Grotjohann, T.; Kapp, D.; Keck, M.; Niehaus, K. Establishment of a high content assay for the identification and characterisation of bioactivities in crude bacterial extracts that interfere with the eukaryotic cell cycle. *J. Biotechnol.* **2009**, *140* (1–2), 124–134.
- (26) Bhattacharyya, S.; Kumar, N. M.; Ganguli, A.; Tantak, M. P.; Kumar, D.; Chakraborti, G. NMK-TD-100, a novel microtubule modulating agent, blocks mitosis and induces apoptosis in HeLa cells by binding to tubulin. *PLoS One* **2013**, *8* (10), e76286.
- (27) Bonne, D.; Heuséle, C.; Simon, C.; Pantaloni, D. 4',6'-Diamidino-2-phenylindole, a fluorescent probe for tubulin and microtubules. *J. Biol. Chem.* **1985**, *260* (5), 2819–2825.
- (28) (a) Kawaratani, Y.; Harada, T.; Hirata, Y.; Nagaoka, Y.; Tanimura, S.; Shibano, M.; Taniguchi, M.; Yasuda, M.; Baba, K.;

Uesato, S. New microtubule polymerization inhibitors comprising a nitrooxymethylphenyl group. *Bioorg. Med. Chem.* **2011**, *19* (13), 3995–4003. (b) Bio, M.; Rajaputra, P.; Nkepan, G.; Awuah, S. G.; Hossion, A. M. L.; You, Y. Site-specific and far-red-light-activatable prodrug of combretastatin A-4 using photo-unclick chemistry. *J. Med. Chem.* **2013**, *56* (10), 3936–3942. (c) Fitzgerald, D. P.; Emerson, D. L.; Qian, Y.; Anwar, T.; Liewehr, D. J.; Steinberg, S. M.; Silberman, S.; Palmieri, D.; Steeg, P. S. TPI-287, a new taxane family member, reduces the brain metastatic colonization of breast cancer cells. *Mol. Cancer Ther.* **2012**, *11* (9), 1959–1967.

(29) Bennani, Y. L.; Gu, W.; Canales, A.; Díaz, F. J.; Eustace, B. K.; Hoover, R. R.; Jiménez-Barbero, J.; Nezami, A.; Wang, T. Tubulin binding, protein-bound conformation in solution, and antimitotic cellular profiling of noscapine and its derivatives. *J. Med. Chem.* **2012**, *55* (5), 1920–1925.